



This is a repository copy of *Hydrogen bonding shuts down tunneling in hydroxycarbenes: a gas-phase study by tandem-mass spectrometry, infrared ion spectroscopy, and theory.*

White Rose Research Online URL for this paper:

<https://eprints.whiterose.ac.uk/208085/>

Version: Accepted Version

Article:

Paul, M., Thomulka, T., Harnying, W. et al. (8 more authors) (2023) Hydrogen bonding shuts down tunneling in hydroxycarbenes: a gas-phase study by tandem-mass spectrometry, infrared ion spectroscopy, and theory. *Journal of the American Chemical Society*, 145 (22). pp. 12124-12135. ISSN 0002-7863

<https://doi.org/10.1021/jacs.3c01698>

© 2023 The Authors. Except as otherwise noted, this author-accepted version of a journal article published in *Journal of the American Chemical Society* is made available via the University of Sheffield Research Publications and Copyright Policy under the terms of the Creative Commons Attribution 4.0 International License (CC-BY 4.0), which permits unrestricted use, distribution and reproduction in any medium, provided the original work is properly cited. To view a copy of this licence, visit <http://creativecommons.org/licenses/by/4.0/>

Reuse

This article is distributed under the terms of the Creative Commons Attribution (CC BY) licence. This licence allows you to distribute, remix, tweak, and build upon the work, even commercially, as long as you credit the authors for the original work. More information and the full terms of the licence here: <https://creativecommons.org/licenses/>

Takedown

If you consider content in White Rose Research Online to be in breach of UK law, please notify us by emailing eprints@whiterose.ac.uk including the URL of the record and the reason for the withdrawal request.



eprints@whiterose.ac.uk
<https://eprints.whiterose.ac.uk/>

This document is confidential and is proprietary to the American Chemical Society and its authors. Do not copy or disclose without written permission. If you have received this item in error, notify the sender and delete all copies.

Hydrogen Bonding Shuts Down Tunneling in Hydroxycarbenes: A Gas-Phase Study by Tandem-Mass Spectrometry, Infrared Ion Spectroscopy, and Theory

Journal:	<i>Journal of the American Chemical Society</i>
Manuscript ID	ja-2023-01698x.R2
Manuscript Type:	Article
Date Submitted by the Author:	n/a
Complete List of Authors:	Paul, Mathias; Universitat zu Koln, Chemistry Thomulka, Thomas; Universitat zu Koln, Chemistry Harnying, Wacharee; Universitat zu Koln, Chemistry Neudörfl, Jörg-Martin; Universitat zu Koln, Institute of Organic Chemistry Adams, Charlie; University of Sheffield, Mechanical Engineering Martens, Jonathan; Radboud Universiteit, FELIX Laboratory Berden, Giel; Radboud Universiteit, Institute for Molecules and Materials Oomens, Jos; Radboud Universiteit, Institute for Molecules and Materials, FELIX Laboratory; University of Amsterdam, Van't Hoff Institute for Molecular Sciences Meijer, Anthony; University of Sheffield, Chemistry Berkessel, Albrecht; Universitat zu Koln, Institut für Organische Chemie Schäfer, Mathias; Universitat zu Koln, Chemistry

SCHOLARONE™
Manuscripts

Hydrogen Bonding Shuts Down Tunneling in Hydroxycarbenes: A Gas-Phase Study by Tandem-Mass Spectrometry, Infrared Ion Spectroscopy, and Theory

Mathias Paul,[†] Thomas Thomulka,[†] Wacharee Harnying,[†] Jörg-Martin Neudörfl,[†] Charlie R. Adams,[‡] Jonathan Martens,[§] Giel Berden,[§] Jos Oomens,^{*,§,#} Anthony J. H. M. Meijer,^{*,‡} Albrecht Berkessel,^{*,†} and Mathias Schäfer^{*,†}

[†]Department of Chemistry, Organic Chemistry, University of Cologne, Greinstraße 4, 50939 Cologne, Germany

[‡]Department of Chemistry, University of Sheffield, Sheffield S3 7HF, U.K.

[§]Radboud University, Institute for Molecules and Materials, FELIX Laboratory, Toernooiveld 7, 6525 ED Nijmegen, The Netherlands

[#]Van't Hoff Institute for Molecular Sciences, University of Amsterdam, Science Park 904, 1098 XH Amsterdam, The Netherlands

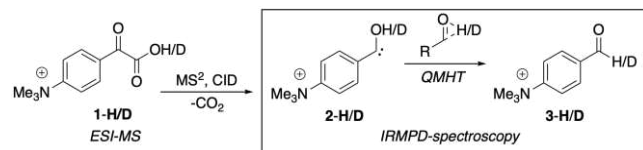
ABSTRACT: Hydroxycarbenes can be generated and structurally characterized in the gas phase by collision-induced decarboxylation of α -keto carboxylic acids, followed by IR ion spectroscopy, IRIS. Using this approach, we have shown earlier that quantum-mechanical hydrogen tunneling (QMHT) accounts for the isomerization of a charge-tagged phenylhydroxycarbene to the corresponding aldehyde, in the gas phase and above room temperature. Herein we report the results of our current study on *aliphatic* trialkylammonio-tagged systems. Quite unexpectedly, the flexible 3-(trimethylammonio)propylhydroxycarbene turned out to be stable - no H-shift to *either* aldehyde *or* enol occurred. As supported by DFT calculations, this novel QMHT inhibition is due to intramolecular H-bonding of the mildly acidic α -ammonio C-H bonds to the hydroxyl carbene's C-atom (C: \cdots H-C). To further support this hypothesis, (4-quinuclidinyl)hydroxycarbenes were synthesized, whose rigid structure prevents this intramolecular H-bonding. The latter hydroxycarbenes underwent "regular" QMHT to the aldehyde, at rates comparable to *e.g.* methylhydroxycarbene studied by Schreiner *et al.*. While QMHT has been shown for a number of biological H-shift processes, its inhibition by H-bonding disclosed here may serve for the stabilization of highly reactive intermediates such as carbenes, even as a mechanism for biasing intrinsic selectivity patterns.

1. INTRODUCTION

The classical concept of chemical selectivity is based on the interplay of thermodynamic and kinetic control, *i.e.* the effects of relative energies and energetic barriers. In contrast, recent years have seen an increasing number of chemical transformations where the selectivity is controlled neither by thermodynamics, nor by classical kinetics, but by quantum-mechanical tunneling.^{1,2,3} The importance of this effect for chemical reactions has recently been emphasized by P. R. Schreiner by naming tunneling control "the third reactivity paradigm".⁴ Tunneling effects in chemical reactions are not limited to hydrogen, but transpositions of H-atoms are the most common ones, due to the low mass of hydrogen and the resulting larger de Broglie wavelength.^{1,2,5} Spectroscopic proof for quantum-mechanical hydrogen tunneling (QMHT) has mostly been obtained under cryogenic conditions, where thermal reactivity is **negligible**.^{4,7} In 2017, we reported the first spectroscopic proof for QMHT in the gas phase (quadrupole ion trap, QIT), at or above room temperature.⁸ In this initial study, the charge-tagged phenylglyoxylic acid derivative **1-H** (Scheme 1) was transferred to the gas-phase by electrospray ionization (ESI). Upon collisional activation, the α -keto acid **1-H** loses CO₂ and delivers the charge-tagged phenyl hydroxycarbene **2-H**. The structure of the latter

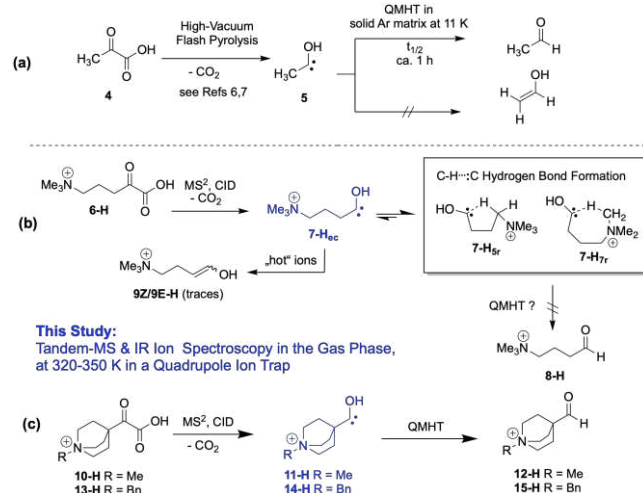
was secured by IR ion spectroscopy (IRIS), based on infrared multiple photon dissociation (IRMPD), in combination with density functional theory (DFT) calculations. Under these experimental conditions (gas phase, ca. 320-350 K), the hydroxycarbene **2-H** isomerizes to the aldehyde **3-H** with $t_{1/2} \approx 10$ s, while its D-isotopologue **2-D** does not appreciably isomerize over the time frame of the experiment, suggesting a Kinetic Isotope Effect (KIE) of more than 20.⁸ Subsequently, a homologous charge-tagged phenylpyruvic acid derivative was investigated by tandem-MS, infrared (IR) ion spectroscopy and theory. Surprisingly, we could not find any evidence of tunneling control.⁹ Our experimental results and extensive DFT computations suggested the intermediate generation of hydroxycarbene products, which in turn rearrange in a secondary process to the enol ions detected by IR ion spectroscopy. Later, the results were scrutinized by semi-classical transition state theory calculations by Burd *et al.* which indicate that tunneling is still a significant factor in the decay of phenylpyruvic acid derivative carbenes, despite the wider, lower barrier being preferred.¹⁰ These calculations elucidated the dynamic behavior of selected hydroxycarbenes, and the computations gave qualitative insight into the temperature-dependence of changes in reactivity.

Scheme 1. Generation of the charge-tagged phenylhydroxycarbene **2** in the gas-phase, and its transformation to the aldehyde **3** by QMHT.



The parent hydroxycarbene,¹¹ methylhydroxycarbene,¹² phenylhydroxycarbene,¹³ and a whole series of further hydroxycarbene¹⁴⁻¹⁶ have been studied by Schreiner *et al.*. Their method of hydroxycarbene generation rests on high-vacuum flash pyrolysis (HVFP) of α -keto carboxylic acids, deposition of the decarboxylation product(s) in cryogenic matrices, and absorption IR spectroscopic analysis of structures and reactivities. For example, methylhydroxycarbene **5** was generated by HVFP of pyruvic acid **4** (Scheme 2, a).¹² In a solid Ar matrix at 11 K, the hydroxycarbene **5** isomerized exclusively to acetaldehyde with $t_{1/2} \approx 1$ h. This result is particularly intriguing because vinyl alcohol, the acetaldehyde enol, is in fact the kinetic product of the hydroxycarbene (**5**) isomerization - which, however, was not formed. In other words, this experiment not only proved that the isomerization of the hydroxycarbene **5** proceeds by QMHT, but it additionally and impressively demonstrates how the selectivity of chemical processes can be steered by QMHT.⁴

Scheme 2. (a) Generation and QMHT-controlled isomerization of methylhydroxycarbene (**5**); (b) charge-tagged α -ketopentanoic acid **6-H** for the generation and study of the hydroxycarbene **7-H_{ec}** with an extended-chain structure in the gas-phase; (c) bicyclic α -keto acids **10,13-H** for the generation of the rigid hydroxycarbene **11,14-H**.



Our gas-phase study on the arylhydroxycarbene **2-H/D** (Scheme 1) did not involve any bias regarding product constitution - only the aldehyde **3-H** could result from H-shift in the hydroxycarbene **2-H**. Intrigued by the above matrix experiments by Schreiner *et al.* on methylhydroxycarbene (**5**), we decided to extend our approach to charge-tagged *aliphatic* α -keto acids, such as the α -ketopentanoic acid derivative **6-H**, the precursor for the gas-phase generation of the hydroxycarbene **7-H** and its characterization by tandem-MS upon collision induced

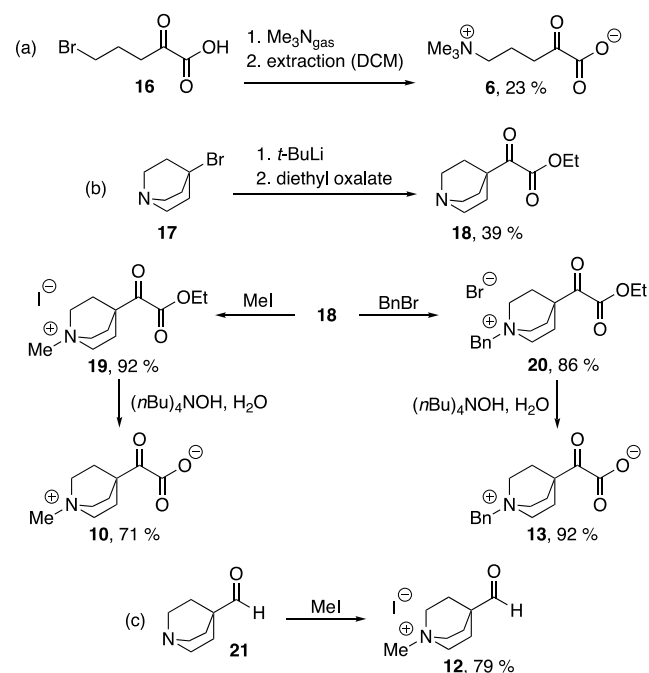
dissociation, CID (Scheme 2b). The tandem-MS and IRIS experiments in a quadrupole ion trap, (QIT) unambiguously confirmed the formation of the *aliphatic* hydroxycarbene **7-H**. However, to our surprise, this hydroxycarbene **7-H** showed exceptional stability in the gas phase, and did not undergo any H-shift - neither to the aldehyde (**8-H**), nor to the enols **9Z/E-H**. With the aid of quantum-chemical calculations and the structurally rigid analogues **11-H**, **14-H** (Scheme 2c) of the hydroxycarbene **7-H**, we were able to identify the source of inhibition in **7-H**. We attribute this unprecedented effect to intramolecular C...H-C hydrogen bonding of the mildly acidic α -ammonio hydrogen atoms to the hydroxycarbene's C-atom, resulting in either 5-membered (**7-H_{5r}**) or 7-membered ring (**7-H_{7r}**) structures (see box in Scheme 2b). This is the first direct observation of intramolecular carbene stabilization by H-bonding, potentially having far-reaching implications for reactivity steering of such highly reactive intermediates, and as a mechanism for biasing intrinsic selectivity patterns.

2. RESULTS AND DISCUSSION

2.1 Synthesis of charge-tagged aliphatic α -keto acids (**6-H**, **10-H**, **13-H**, and of the aldehydes **12-H**, **15-H** as reference compounds

For our synthesis of 5-trimethylammonio-2-oxopentanoic acid (**6-H**), the known 5-bromo-2-oxopentanoic acid (**16**) served as the starting material (Scheme 3a).¹⁷ Treatment with gaseous trimethylamine resulted in the formation of a mixture of the neutral zwitterion **6** with trimethylammonium bromide. The latter byproduct could be removed by extensive washing with dichloromethane DCM (see the Supporting Information for details of the synthesis and characterization of the zwitterion **6**, including its X-ray crystal structure).

Scheme 3. Preparation of charge-tagged α -ketocarboxylic acids in zwitterionic form: (a) 5-trimethylammonio-2-oxo-pentanoate **6**; (b) (*N*-methyl-4-quinuclidinio)glyoxylate **10** and (*N*-benzyl-4-quinuclidinio)glyoxylate **13**; (c) quinuclidinium aldehyde **12**.



For the synthesis of the quinuclidinium-derived zwitterions **10** and **13**, known 4-bromoquinuclidine (**17**) served as the starting material (Scheme 3b).¹⁸ Treatment of the latter with *tert*-butyl lithium, followed by diethyl oxalate gave the 4-quinuclidinio glyoxylate **18**. Both N-methylation and N-benylation of this intermediate proceeded smoothly and gave the quinuclidinium salts **19** and **20**. Hydrolysis of the latter effected by tetra-*n*-butyl ammonium hydroxide completed the synthesis of the zwitterions **10** and **13**, respectively (see the Supporting Information for details of the synthesis and characterization of the zwitterions **10** and **13**, including the X-ray crystal structure of **10**). Finally, the charge-tagged quinuclidinium aldehyde **12**, needed as reference compound, was readily available by *N*-methylation of the known 4-formylquinuclidine **21** (Scheme 3c).¹⁹

2.2 Gas-phase studies on the aliphatic α -keto acids **6-H**, **10-H** and **13-H**

For ESI-MS experiments, the charge-tagged α -keto acids **6-H**, **10-H** and **13-H** were generated in situ, by dissolving the zwitterions **6**, **10** and **13**, respectively, in methanol as spray solvent, containing a small amount of formic acid. Similar to previous studies, we used infrared ion spectroscopy experiments to elucidate and assign individual isobaric conformer and tautomer ion structures in a QIT.^{8,20} Gaseous ions were generated from respective analyte solutions by conventional (+)-ESI, and the ions of interest were probed in a modified 3D-QIT mass spectrometer.^{8,20} Once generated and selected in the QIT, ions were photo-activated with radiation from a wavelength-tunable free electron laser (FEL) and with light from an optical parametric oscillator (OPO) laser as described earlier.²¹ The extent of precursor ion depletion and fragment ion formation was monitored as the energy of the photons used for activation was tuned (FEL: from 600 to 1800 cm^{-1} and OPO: 2800–3700 cm^{-1}). The infrared multiple-photon dissociation (IRMPD) ion spectroscopy applied here at RT relies on intramolecular vibrational redistribution (IVR) of the energy of tens to hundreds of resonantly absorbed photons, which leads to a global vibrational excitation of all oscillators in the ion until critical threshold energies for dissociation pathways are reached and photo-fragments are observed.²² IR ion spectra thus obtained are interpreted by comparison with computed linear IR spectra of ion structures provided by theory. This combination of IR ion spectroscopy with theory has proven to be an efficient and reliable strategy for the detailed analysis of ion structures.^{8,20,22f, 22g}

2.2.1 Structural characterization of the α -keto carboxylic acid **6-H**

When applied to the parent ion of the α -keto carboxylic acid **6-H** (m/z 174), the comparison of calculated IR-spectra at the dispersion-corrected B3LYP-D3(BJ)/cc-pVTZ level of theory with those obtained from IRIS experiments clearly confirmed the intact structure of **6-H** as shown in Scheme 2b (see Figures S25-S27, SI). There appears to be no H-bond between the carboxyl O-H and the O-atom of the neighboring keto function. In fact, the structure assigned to **6-H** in the gas phase is virtually identical to the one found by X-ray crystallography for the bromide salt of **6-H** (see Figure S16, S50, SI). Similarly, no indications for enolization were obtained.

2.2.2 CID-Decarboxylation of the aliphatic α -keto carboxylic acid **6-H**, reactivity of the resulting hydroxycarbene **7-H**

CID of the molecular ion of **6-H** at m/z 174 resulted in the loss of CO_2 and provided an abundant fragment ion at m/z 130 of $[\text{C}_7\text{H}_{16}\text{ON}]^+$ composition, entirely consistent with our extensive examination of the respective potential energy surface (see Figures S19 and S46, SI). For structure determination, the CO_2 -loss product ion at m/z 130 was probed by IRIS. In analogy to our earlier investigation of the ketocarboxylic acid **1-H** (Scheme 1), we expected to see the IR-signature of the hydroxycarbene **7-H** and the further conversion of the hydroxycarbene to either the aldehyde **8-H**, or to the enols **9Z/E-H** (Scheme 2b; see Figures S29-S32, SI). The experimentally obtained IR-spectrum is shown in Figure 1, together with computed linear IR spectra of ion structures identified by theory. As the most striking aspect, the experimental IR-spectrum *does not show any trace* of the typically strong stretching vibration $\nu \text{C}=\text{O}$ of the carbonyl functionality of aldehyde **8-H**, which is calculated to be around 1750 cm^{-1} (see Figure S31). This remarkable result indicates the absence of the expected H-tunneling product of hydroxycarbene **7-H**, *i.e.* the aldehyde **8-H**. The very weak band at 1660 cm^{-1} , matching the alkenol stretching vibration $\nu \text{C}=\text{COH}$ of the enol(s) **9Z/E-H** (Scheme 2), points towards the presence of these tautomers (compare Figure S35, SI). However, the intensity of this weak band was time-invariant, and independent of whether the α -keto carboxylic acid **6-H** or its isotopologue **6-D** was used, *i.e.* a KIE was not detected. The latter observation points towards formation of the enol tautomer, as the kinetic 1,2-H-shift product, via the “classical” thermal pathway, most likely originating from a small portion of thermally non-equilibrated **7-H** ions present after CID (see Figure S32 and S37, SI).⁹

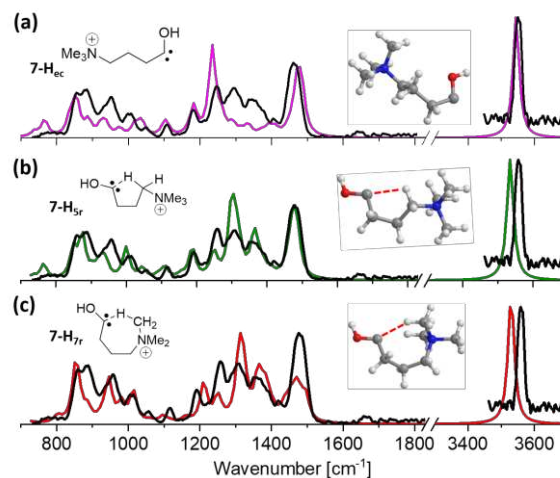


Figure 1. IR-ion spectrum of the CO_2 -loss product ion at m/z 130 (black trace) compared with the calculated, linear IR spectra of three structural alternatives for the hydroxycarbene ion **7-H**: (a) hydroxycarbene conformer with an extended propyl chain (**7-H_{ec}**; +223.2 kJ mol^{-1}), pink trace; (b) hydroxycarbene with intramolecular C \cdots H-C H-bonding (orange dotted line), resulting in a 5-membered ring (**7-H_{5r}**; +208 kJ mol^{-1}), green trace; (c) ditto with intramolecular H-bonding (orange dotted line), resulting in a 7-membered ring (**7-H_{7r}**; +214 kJ mol^{-1}), red trace. All zero-point corrected relative energies vs. aldehyde **8-H** (see Figure 2). The band positions of the computed hydroxycarbene ground state structure, **7-H_{5r}**, are summarized in Table S2 (SI). The intensity in the wavenumber range 3500–3700 cm^{-1} covered by the OPO-laser is normalized to the signal intensity predicted by theory.

Thus, the species at m/z 130 obtained upon CID-decarboxylation of the α -ketocarboxylic acid **6-H** is remarkably *stable* under our experimental conditions, in the gas phase at ca. 320-350 K.⁸ On the other hand, the IR spectra obtained from the decarboxylation product clearly identify it as a hydroxycarbene: the strong O-H stretching mode ν O-H at 3560 cm^{-1} and the characteristic stretching vibration of the C-OH bond, *i.e.* the ν C-OH band at 1305 cm^{-1} are particularly indicative. Thus, how can it be possible that the hydroxycarbene produced from the aliphatic α -ketocarboxylic acid **6-H** is unreactive, while methylhydroxycarbene (**5**, Scheme 2) readily undergoes QMHT to acetaldehyde, even in an Ar-matrix at 11 K?¹² We found the solution to this riddle in intramolecular C \cdots H-C hydrogen bonding. C-H bonds adjacent to an ammonium cation are substantially polarized, making the respective hydrogen atoms mildly acidic. It is known that such hydrogen atoms form H-bonds to centers of high electron density.²³ In hydroxycarbene **7-H**, intramolecular interaction of C-H bonds α to the ammonium cation with the carbene C-atom may result in the formation of either a 5-membered (**7-H_{5r}**, Scheme 2b and Figure 1b) or a 7-membered (**7-H_{7r}**, Scheme 2b and Figure 1c) ring structure. In Figure 1, the experimental IR-spectrum is compared with the one calculated for the extended-chain structure **7-H_{ec}** of the hydroxycarbene **7-H** (Figure 1a), and with the two cyclic, C \cdots H-C hydrogen-bonded ones (**7-H_{5r}**, Figure 1b; **7-H_{7r}**, Figure 1c). In line with the mildly exothermic character of H-bonding found for these species, the structure of the hydroxycarbene **7-H** is best represented by the 5-membered ring **7-H_{5r}** (Figure 1b). In the latter, C \cdots H-C H-bonding suppresses the QMHT reactivity of the hydroxycarbene. Note that we also considered various options of H-bonding to and from the hydroxyl group of the carbene **7-H**, as well as alternative hydroxyl-hydrogen conformers (see Figure S30, SI).¹⁵ None of the IR-spectra computed for such species matches the experimental one better than **7-H_{5r}** or **7-H_{7r}** (see Figures S29-S34, SI). **Finally, we considered intramolecular carbene insertion reactions into one of the C-H bonds of **7-H** to form covalently bound cyclic ion structures, although this is a spin-selective process which is limited to triplet carbenes.**²⁴ Accordingly, the precursor **7-H_{5r}** would give rise to four membered ring products, *i.e.* E- or Z-2-*N,N,N*-trimethylammonium cyclobutanol, while **7-H_{7r}** would give rise to 3-hydroxy-*N,N*-dimethyl-piperidinium ions. The respective diastereomers of 2-*N,N,N*-trimethylammonium cyclobutanol as well as both conformers of 3-hydroxy-*N,N*-dimethyl-piperidinium are computed and their linear IR ion spectra are evaluated (see Figures S35 and S36, SI). The clearly less convincing agreement with the recorded spectrum of the CO₂ loss product allows discarding these alternative ion structures and the C-H insertion process.

The pathways of tautomerization, from the three forms of the hydroxycarbene **7-H** (**7-H_{ec}**, **7-H_{5r}** and **7-H_{7r}**) to the aldehyde **8-H** and the enols **9Z/E-H** were analyzed computationally, and the results are summarized in Figure 2. Analogous to methylhydroxycarbene **5**,¹² the aldehyde **8-H** is the thermodynamic product, while the enols **9Z/E-H** are kinetically favored. For the “extended chain” form of the hydroxycarbene **7-H** (**7-H_{ec}**; Figure 2, right), an energetic profile results that is reminiscent of that reported by Schreiner *et al.* for methylhydroxycarbene **5**, leading to the **9Z-H** enol.¹² However, the energetically most favorable form of our hydroxycarbene **7-H** is its H-bonded 5-membered ring in the singlet state, *i.e.* **7-H_{5r}** (Figure 2, middle). Relative to the extended-chain form **7-H_{ec}**, a stabilization of ca. 14 kJ mol⁻¹ results, together with an increase in the energy of the

transition state of tautomerization of ca. 8 kJ mol⁻¹ for both directions of tautomerization. All hydroxycarbene ion structures discussed in this study are in their singlet state, as the respective triplets are energetically not competitive (see details in the Experimental Part on Computations). It will be discussed later whether ground-state stabilization alone may account for tunneling inhibition, or whether other quantum-mechanical effects result from H-bonding to the carbene center (see section 2.3).

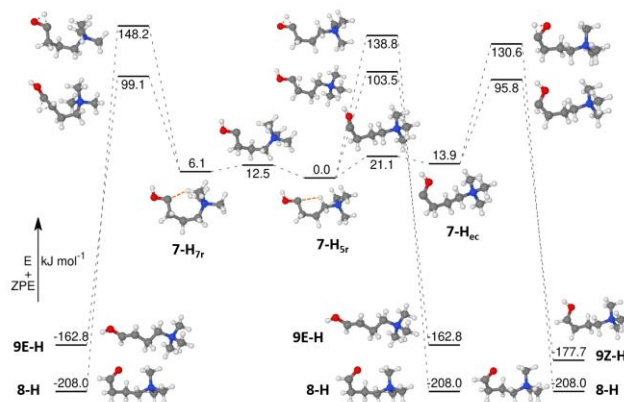


Figure 2. Energy profiles computed for the tautomerization of the hydroxycarbenes **7-H_{ec}**, **7-H_{5r}** and **7-H_{7r}**, showing the transition states for the 1,2-hydrogen shift reactions to the aldehyde **8-H** and the enol diastereomers **9Z/E-H**, as well as the barrier-free formation of the H-bond stabilized hydroxycarbenes **7-H_{5r}** and **7-H_{7r}** from the extended-chain form **7-H_{ec}**. Note that the **7-H_{ec}** conformer shown in the energy profile and in Figure 1 lies +4.9 kJ mol⁻¹ above the lowest all *anti*-conformer of **7-H_{ec}** (see Scheme 2 and Figure S29, SI). All structures were optimized using dispersion-corrected B3LYP-D3BJ/cc-pVTZ, while energies were calculated at CCSD(T)-F12//cc-pVDZ. Zero-point energy corrections were calculated at the B3LYP-D3BJ/cc-pVTZ level of theory.

Tautomer-selective IR kinetics of the conversion of the hydroxycarbene **7-H/7-D** were conducted and are presented in Figure 4. To safeguard for the necessitated precursor ion selectivity, the kinetic study was conducted at the photon energy of the carbene ν C-OH stretching mode at 1305 cm^{-1} at which the carbene absorbs while the respective aldehyde **8-H** is transparent (see Figure S31, SI). Introduction of a time delay between formation of **7-H** and IRMPD interrogation of up to 20 s, did not indicate any substantial conversion of the hydroxycarbene **7-H** (see Figure 4 for the FELIX time/intensity profiles recorded for both the hydroxycarbene **7-H** and its isotopologue **7-D**) or delayed formation of **8-H** either, and therefore no QMHT half-life $t_{1/2}$ was determined.

2.2.3 CID-Decarboxylation of the quinuclidyl α -keto carboxylic acid **10-H**, reactivity of the hydroxycarbenes **11-H**

As “positive probes” for our hypothesis that intramolecular C \cdots H-C H-bonding suppresses QMHT in the hydroxycarbene **7-H_{5r}**, we envisaged the generation and examination of 4-quinuclidinium substituted hydroxycarbenes, such as **11-H** and **14-H** shown in Scheme 2c. In the latter, the number of C-atoms separating the hydroxycarbene moiety from the ammonium tag is identical to the one present in the acyclic hydroxycarbene **7-**

H (three C-atoms). However, the rigidity of the bicyclic quinuclidinium core securely prevents the interaction of any of the C-H bonds α to the ammonium cation with the carbene C-atom.

Again, the α -keto-carboxylic acids **10-H** (*N*-methyl) and **13-H** (*N*-benzyl) served as the precursors for the generation and examination of the corresponding charge-tagged hydroxycarbenes (**11-H** and **14-H**, respectively, Scheme 2). (+)ESI-MS smoothly provided the molecular ions of both carboxylic acids for tandem-MS (Figure S20 and S22, SI). The intactness of the α -keto-carboxylic acid structure of the *N*-methylquinuclidinium α -keto-carboxylic acid **10-H** was exemplarily proven by IRMPD spectroscopy of the ion at m/z 198 and comparison with calculated spectra (see Figures S38-S39, SI). When the molecular ion of **10-H** was subjected to CID, loss of CO₂ resulted in the abundant formation of a fragment ion at m/z 154 (Figure S20, SI). Its IR ion spectrum is shown in Figure 3a, together with the IR spectrum calculated for the hydroxycarbene **11-H**. Figure 3a additionally shows the IR spectrum calculated for the QMHT product, the aldehyde **12-H**, and the experimental IR spectrum obtained by IRMPD from the authentic reference aldehyde **12-H**. The potential energy surfaces of **10-H** and **12-H** were fully computed and are presented in the Supporting Information (see Figures S47-S49, SI).

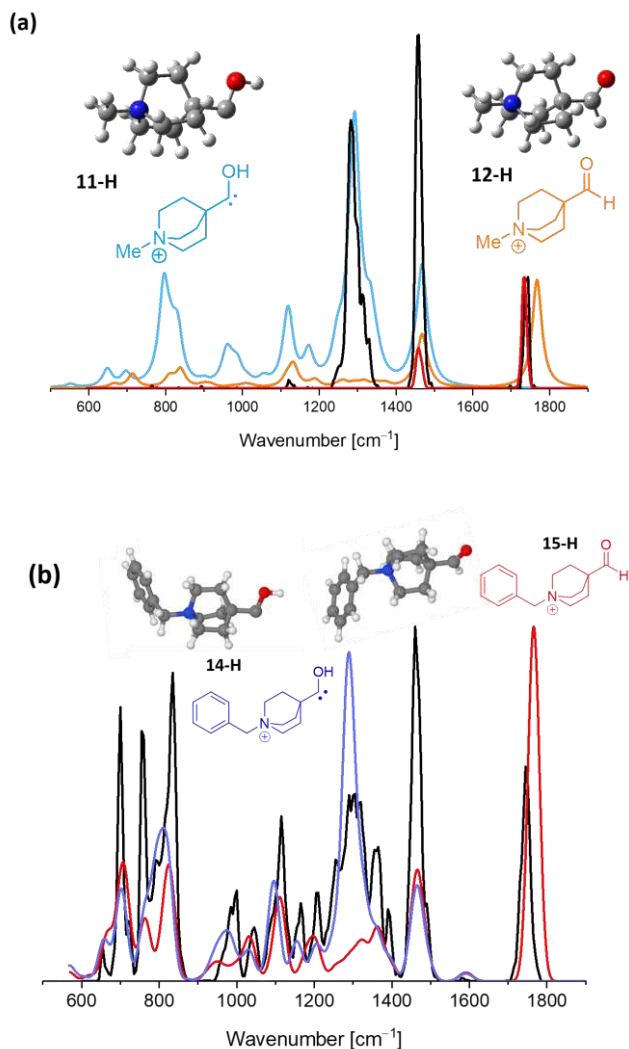


Figure 3. (a) IR ion spectrum of the CO₂-loss product ion at m/z 154 (black trace) produced from **10-H** upon CID compared with the calculated, linear IR spectrum of the hydroxycarbene ion **11-H** (+195 kJmol⁻¹; blue trace), together with the computed IR-spectrum of the aldehyde **12-H** (0 kJmol⁻¹; orange trace), and the experimental spectrum of the reference aldehyde **12-H** (red trace). (b) IR ion spectrum of the CO₂-loss product ion at m/z 230 (black trace) produced from **13-H** upon CID compared with the calculated, linear IR spectrum of the hydroxycarbene ion **14-H** (+197 kJmol⁻¹; blue trace), together with the computed IR-spectrum of the aldehyde **15-H** (0 kJmol⁻¹; red trace). The band positions of the computed hydroxycarbene structure **11-H** and **14-H** are summarized in Tables S3 and S4 (SI).

Figure 3a clearly demonstrates that the product resulting from the decarboxylation of the bicyclic α -keto-carboxylic acid **10-H** is in fact the quinuclidinylhydroxycarbene **11-H** exhibiting the characteristic stretching vibration of the C-OH bond, *i.e.* the ν C-OH band at 1280 cm⁻¹. Furthermore, the calculated O-H stretching band ν O-H band at 3544 cm⁻¹ is perfectly matching the experimental band as documented in Figure S40 (SI). In Figure 3a, the carbonyl band of the aldehyde **12-H** (at 1740 cm⁻¹), resulting from QMHT in the carbene **11-H**, is clearly visible. The introduction of a delay before the IRMPD measurement led to an increase of the aldehyde concentration with time (see Figures S50-S51, SI), and allowed the half-life of the hydroxycarbene **11-H** to be estimated as ca. 5 s. Note that this value is in the same range as the half-life determined earlier by us for the hydroxycarbene **2-H** in the gas phase, namely 10 s.⁸ When the deuterated hydroxycarbene **11-D** was generated from the deuterated α -keto-carboxylic acid **10-D**, no increasing formation of aldehyde with time was observed (see Figures S42 and S54-S55, SI).

It needs to be mentioned at this point that the measurement of the tautomer-selective kinetics of the hydroxycarbene **11-H** proved unusually difficult. The *N*-methylquinuclidinium tag showed unexpectedly high stability towards multiple-photon dissociation, ultimately resulting in many low-abundance fragments (Figure S43-S45, SI). To eliminate this problem, we additionally included the *N*-benzylquinuclidinium α -keto carboxylic acid **13-H** in our study. Again, collisional activation of its parent ion (m/z 274) induced smooth decarboxylation to the hydroxycarbene **14-H** (m/z 230), as shown in Figure 3b (see also Figures S22-S24, SI). The latter proved ideally suited for IRMPD measurements, as clean debenzylation delivered the stable and abundant [C₇H₇]⁺ product ion at m/z 91 upon multiple-photon excitation similar to CID (see Figure 5 and Figures S22-S24, SI).

Consequently, we were able to cleanly follow the conversion of the hydroxycarbene **14-H** to the aldehyde **15-H** (Figure 4, top). Note that this is actually a “two-channel” kinetic measurement: here, not only the decay of the hydroxycarbene **14-H** was individually monitored on the basis of the progressive depletion of the ν C-OH stretching mode at 1300 cm⁻¹, but also the time-dependent emergence of the aldehyde **15-H** could be monitored on the basis of the ν C=O stretching mode at 1744 cm⁻¹. From both kinetic curves, the half-life of the hydroxycarbene **14-H** was deduced to be ca. 3 s (compare kinetic data analysis in Figures S56 and S57, SI). When the O-deuterated hydroxycarbene **14-D** was generated from the corresponding α -ketoacid **13-D**, only minute conversion to the aldehyde **15-D** could be observed within the time frame of the experiment (delay time up to 16 s;

Figure 4, bottom). The half-life of **14-D** was deduced to be around 19 s. The respective KIE of the *N*-benzylquinuclidine model compounds is found to be around 8 (Figure S57, SI).

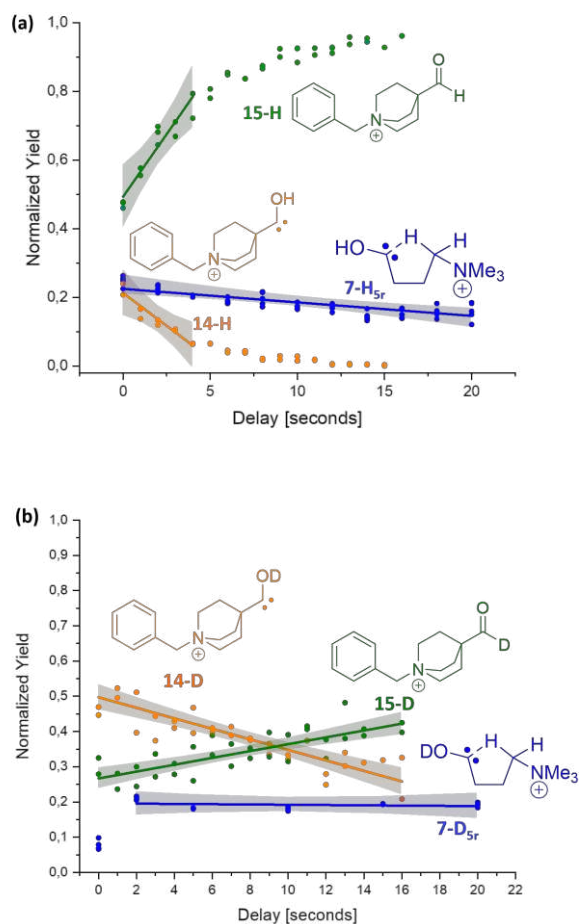


Figure 4. (a) Tautomer-selective IR kinetics of the hydroxycarbenes **7-H** and **14-H** and (b) their O-deuterated isotopologues **7-D** and **14-D**. The kinetic studies were conducted at individual photon energies at which the carbenes absorb (ν C-OH stretching mode) and the aldehydes are transparent, and *vice versa* (ν_{as} C=O stretching mode). The IR spectra of **7-H** (see Figure 1) and **7-D** (see Figure S33, SI) show no evidence for any aldehyde formation and hence, the formation of the respective aldehydes **8-H** or **8-D** is not represented in the kinetic plots. The normalized ion yields of **7-D_{5r}** without any delay were not included in the fit. The IRMPD reaction of **7-H/D** to ammonium NH_4^+ was used for the measurements as Figure S51 illustrates (see SI). The individual data sets were fitted linearly and 95% confidence intervals are included.

The reaction energy profile for the 1,2-H shift in the hydroxycarbene **14-H** was calculated and is shown in Figure 5. In **14-H**, there is no bias regarding enol formation. Therefore, the overall reaction profile is relatively simple. From the *s*-trans configured energetic ground state of the hydroxycarbene **14-H**, the thermal barrier to aldehyde formation amounts to ca. 130 kJ mol⁻¹. Loss of $[\text{C}_7\text{H}_7]^+$ is the preferred fragmentation channel, which yields the respective aldehyde **15-H**, a result that was similarly found for IRMPD of the aromatic hydroxycarbene

2-H.⁸ An alternative decarbonylation reaction would require a substantially higher activation energy of ca. 250 kJ mol⁻¹ - unsurmountable under our experimental conditions of ca. 320-350 K.

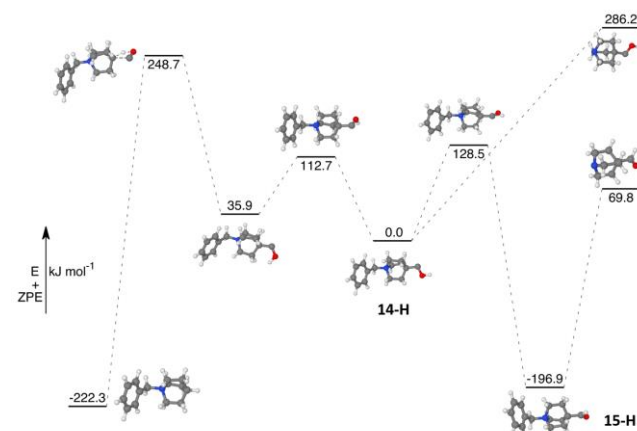


Figure 5. Energy profile computed for the tautomerization of the hydroxycarbene **14-H**, showing the transition states for the 1,2-hydrogen shift reaction to the aldehyde **15-H** and for thermal decarbonylation of the hydroxycarbene **14-H**. Note that the prominent loss of $[\text{C}_7\text{H}_7]^+$ observed upon IRMPD and CID follows formation of aldehyde **15-H**. All structures were optimised using dispersion-corrected B3LYP-D3BJ/cc-pVTZ, while energies were calculated with CCSD(T)-F12//cc-pVDZ. Zero-point energy corrections were calculated at the B3LYP-D3BJ/cc-pVTZ level of theory.

2.2.4 Summary of the gas-phase reactivities observed for the aliphatic hydroxyl carbenes **7-H** and **11/14-H**

The structurally rigid aliphatic hydroxycarbenes **11-H** and **14-H** efficiently undergo tautomerization to the corresponding aldehydes. O-Deuteration completely shuts down this reactivity channel, indicating QMHT. In other words, the rigid aliphatic hydroxycarbenes **11-H** and **14-H** behave in the gas phase in a manner analogous to their “minimalistic” counterpart methylhydroxycarbene (**5**), for which QMHT activity was shown by Schreiner *et al.* under cryogenic conditions.³ In contrast, the acyclic hydroxycarbene **7-H** is stable under the current experimental condition, *i.e.* in the gas phase at ca. 320-350 K.⁸ While the intact hydroxycarbene substructure is maintained, the inhibition of QMHT results from the intramolecular C: \cdots H-C hydrogen bonding interaction of the carbene C-atom with an α -ammonio C-H bond. H-Bonding with a singlet carbene acting as the Lewis base has been observed numerous before in an intermolecular fashion, with a broad variety of impacts on stability and reactivity of the respective carbenes.^{23,25} Our results evidence that the unique *intramolecular* C: \cdots H-C hydrogen bonding interaction stabilizing both **7-H_{5r}** / **7-H_{7r}** ions governs the shut-down of the [1,2]H-shift from the OH group. We note that the QMHT product, *i.e.* aldehyde **8-H** is also stabilized by a more conventional intramolecular hydrogen bond C=O: \cdots H-C between the carbonyl oxygen and a polarized methylene hydrogen (see Figure S31, SI). As a consequence of the carbene stabilization upon C: \cdots H-C interaction, the barrier height and width of the QMHT path between **7-H_{5r}** / **7-H_{7r}** and **8-H** is increased leading to a substantially prolonged QMHT half-life. This finding is complementary with the stabilizing influence of Lewis basic solvents/matrix materials on methyl hydroxycarbene in cryogenic solid-state spectroscopy.^{3,7,12}

Furthermore, the stabilizing C \cdots H-C intramolecular hydrogen bond in **7-H_{7r}** and **5r** ions leads to enlarged energy gaps between relevant quantum states in **7-H_{7r}** and **7-H_{5r}** ions vs. those in the **7-H_{ec}** ions with an extended chain. This in turn could explain hampered energy dissipation processes in **7-H_{7r}** and **7-H_{5r}** ions between initially occupied quantum states and those that are appropriate for QMHT as discussed for phonon excitations in cryogenic solids.^{12,26} In this context, it is important to note that energy dissipation is in any case more difficult at reduced pressures in the gas phase, leading to decreased QMHT rates, than it is in the solid state, as evidenced with experiments at cryogenic temperatures in frozen noble gas matrices.^{4a,7,12} In the gas phase, the energy dissipation in the tunneling ions happens by virtue of many low-energy collisions with the light He atoms during isolation and storage.²⁷ The presence of the helium buffer gas at mTorr pressures in QIT instruments used for our experiments safeguards for ion thermalization with - at least roughly - defined effective internal ion temperatures.⁸ However, the influence of the He pressure on tunneling rates in the gas phase of ion traps remains to be thoroughly investigated.²⁸

2.3 Semi-classical calculations on the reactivity patterns and tautomerization kinetics of the hydroxycarbene **7-H**, **11/14-H** and of methylhydroxycarbene (**5**)

The kinetic data clearly shows the importance of QMHT or the absence thereof in the tautomerization kinetics of the hydroxycarbene **7-H**, **11/14-H** towards the corresponding aldehydes, warranting a closer look at the dynamics underpinning these processes beyond the height of the various barriers.

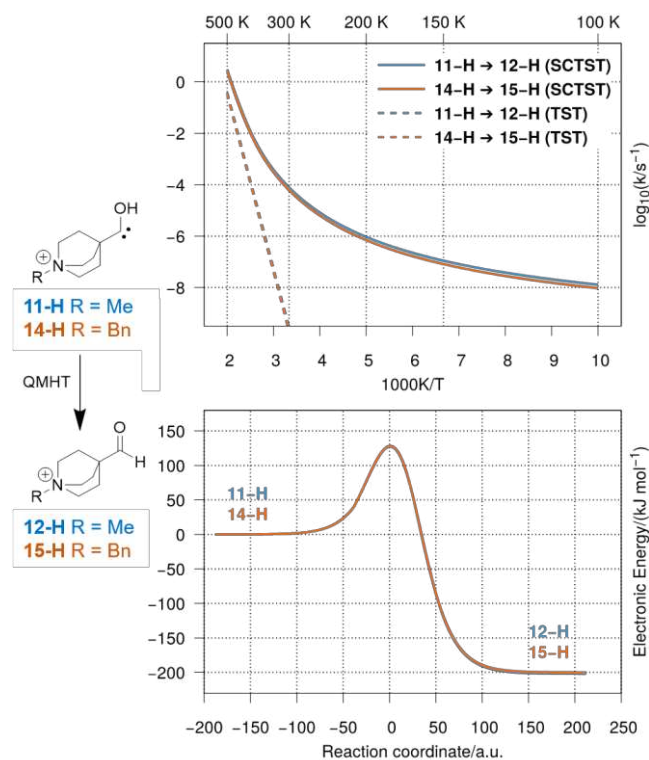


Figure 6: Top panel Arrhenius plot: Tunneling rates for hydroxycarbene **11-H** and **14-H** towards the formation of aldehydes **12-H** and **15-H**, respectively. Classical transition state (TST) theory results shown as dotted lines. The bottom panel

shows the barrier towards formation of the aldehydes **12-H** and **15-H**. Please note that the similarity of the barriers delivers only a single visible curve.

To this end, we performed rate calculations for the tautomerization processes using semi-classical transition state theory (SCTST).^{29,30} Thus, tunneling probabilities (and from these, thermal rate constants) were calculated analytically using the WKB (semiclassical) wavefunction combined with vibrational perturbation theory using SCTST in its one-dimensional form (1D-SCTST). In these calculations, the reaction mode was considered separable from the other (bound) degrees of freedom, allowing a focus on just the tunneling of the hydrogen atom. Our calculations use an adapted version of the pySCTST code³¹ to take account of variations in the local python libraries. Therefore, to benchmark and test the code calculations on the methylhydroxycarbene **5** were performed first. These results are presented in Figure S58 (SI) and show excellent agreement with the results from Burd *et al.*¹⁰ and Meisner^{1d} indicating that the change in functional and basis set does not have a significant impact on the reported rate of tautomerization. To summarize for the methylhydroxycarbene **5** the aldehyde should dominate at low temperatures and the enol at higher temperatures, with a cross-over point around 285 K.^{3,12} The good agreement with previous work allowed us to study our systems and be confident of the accuracy of the results. Our results for the aromatic hydroxycarbene **2-H** are given in Figure S59 (SI). The computations clearly confirm our previous findings in that the barriers towards formation of the aldehyde **3-H/D** differ substantially. The barrier as a function of mass-weighted coordinates is predicted to be much broader for the 1,2-D shift compared to the ¹H case, nicely explaining a minimal tunneling rate of **2-D** and a substantially prolonged half-life.⁸

The results for the aliphatic compounds **11-H** and **14-H** are given in Figure 6.

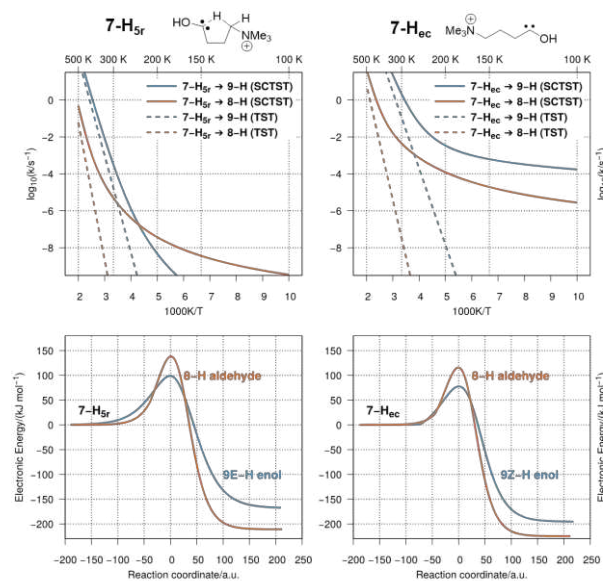


Figure 7: Top row Arrhenius plot: Tunneling rates for hydroxycarbene **7-H_{5r}** towards the formation of aldehyde **8-H** and enol **9E-H** (left panel) and for hydroxycarbene **7-H_{ec}** towards the formation of **8-H** and **9E-H** (right panel). TST theory results shown as dotted lines. The bottom row shows the corresponding barriers towards formation of the aldehyde **8-H** and enol **9E-H** from **7-H_{5r}** (left panel) and **7-H_{ec}** (right panel).

Comparison of Figure 6 with Figure S59 (SI) shows that the rate of tunneling is similar for all three compounds with a significant contribution of tunneling at any temperature below 400 K. Moreover, the barriers towards formation of the aldehydes **3-H**, **12-H**, and **15-H** from the respective hydroxycarbenes are the same within 1 kJ mol⁻¹ at both B3LYP-D3BJ level and at the CCSD(T)-F12//cc-pVDZ + ZPE(B3LYP-D3BJ//cc-pVTZ) level (reported in Figure 2 of Ref. 8 and Figure 5, respectively). As a consequence, we conclude that all compounds should show similar half times, a conclusion which qualitatively agrees with the experimental findings, where the $t_{1/2}$ for depletion of the hydroxycarbenes was found to be 10 s for **2-H**, 5 s for **11-H** and 3 s for **14-H**. For the latter a $t_{1/2}$ of 3 s was found based on the aldehyde formation as well. We note that the exothermicity for formation of the aldehyde was similar in all cases as well.¹⁴

The results for the tunneling calculations for the formation of the aldehyde **8-H** and enol **9E/Z-H** from the hydroxycarbenes **7-H_{sr}** and **7-H_{ec}** are given in the left and right columns of Figure 7, respectively. Comparison of the two columns shows the effect of the hydrogen-bonding interaction in **7-H_{sr}** relative to **7-H_{ec}** in that the rate for tautomerization is significantly lower for the former than for the latter, both for the TST calculations and for the 1D-SCTST calculations. This is also reflected in the fact that the barrier for the formation of the aldehyde **8-H** and enol **9E-H** from the hydroxycarbene **7-H_{sr}** is significantly higher than the corresponding barriers for forming **8-H** and **9Z-H** starting from the hydroxycarbene **7-H_{ec}**. Comparing the rates starting from each of the isomers of **7-H** with the rate calculated for the tautomerisation of **11-H** and **14-H** as shown in Figure 6, indicates that if **7-H_{ec}** were the correct structure for **7-H** then the rate of aldehyde formation should be 1 order of magnitude faster for **7-H** than for **11-H** or **14-H** (and even faster than the methylhydroxycarbene **5**). It should be noted as well that starting from **7-H_{ec}** the expectation would be that formation of the enol **9E-H** should always be the dominant channel at any temperature. In contrast, starting from **7-H_{sr}** the formation of the enol **9Z-H** is dominant at high temperatures until the crossing point at 250 K is reached. At lower temperatures the aldehyde **8-H** is predicted to be formed similar to the behavior of methylhydroxycarbene **5**, even though in that case the crossover point is at around 285 K (see Figure S58, SI). Finally, it is noted that for the interconversion from **7-H_{sr}** to **9Z-H** tunneling at higher temperatures is less important than for the interconversion from **7-H_{ec}** to **9E-H**. Our assignment of **7-H_{sr}** as the correct structure is therefore in line with our experimental data as presented in Figure 1, where the existence of small amounts of enol **9-H** was found not to depend on tunneling.

3. CONCLUSIONS

In this contribution we report the first description of an intramolecular C \cdots H-C interaction in hydroxycarbene ions in the gas phase, and furthermore prove that this non-covalent bond is responsible for the exceptional QMHT behavior of **7-H_{sr}** / **7-H_{tr}** ions. This important assumption is fundamentally probed with the study of a set of tailor-made quinuclidine model compounds, which are unable to establish this feature. The rigid quinuclidinium ions **11-H** and **14-H** exhibit QMHT as predicted by theory, which convincingly confirms the important finding. To complement the experiments, we perform semi-classical transition state theory computations to predict QMHT rates.

The SCTST computations are consistent with our new results and furthermore complete the data on the aromatic hydroxycarbene **2-H** reported earlier.⁸

We clearly show that QMHT can effectively be inhibited by the formation of intramolecular C \cdots H-C interactions. This implies that the carbene singlet electron pair acts as the acceptor in the [1,2]H-shift mechanism via QMHT. A 1,2-hydride shift via QMHT seems unlikely, because that would be eased upon interaction of the Lewis basic carbene with the Lewis acidic polarized hydrogen in the C \cdots H-C interaction. Hence, our results point towards a proton transfer via QMHT.

In the gas-phase of the QIT, in an observation time frame of up to 20 s, neither the kinetic product nor the thermodynamic product is formed from the **7-H_{sr}** / **7-H_{tr}** ions! At first sight, this finding appears to contradict the third reaction paradigm, *i.e.* tunneling control.⁴ However, the computed rates highlight that QMHT is only vastly retarded and thereby not observed.

Finally, this set of results might also contribute to an improved understanding of the fundamentals of enzymatic QMHT processes in the condensed phase at elevated temperatures.³²

4. EXPERIMENTAL SECTION

4.1. Materials

The charge-tagged zwitterionic α -ketocarboxylic acids **6**, **10**, **13** and the aldehyde **12** were synthesized as summarized in section 2.1 in the Supporting Information.

4.2. Mass Spectrometry

All zwitterionic compounds **6**, **10**, **12** and **13** were dissolved (c $\sim 10^{-5}$ M) in 1 ml CH₃CN or in CH₃OH, and the resulting solutions were acidified with a drop (ca. 2 μ l) of formic acid for (+)ESI-MS, MS² and subsequent IR ion spectroscopic analysis. For the analysis of the monodeuterated hydroxycarbenes **7-D**, **11-D** and **14-D**, the respective α -ketocarboxylic acid precursors **6**, **10** and **13** were dissolved in acidified (formic acid) CD₃OD for H/D exchange of the acidic protons prior to (+)ESI-MS. All (+)ESI, tandem-MS and accurate ion mass measurements were conducted on an LTQ-Orbitrap XL instrument (ThermoFisher, Bremen Germany). Accurate ion mass measurements were executed in the orbitrap analyzer with a resolution of 30000 fwhm with external calibration ($\Delta m < 2$ ppm) or with addition of internal standards ($\Delta m < 1-2$ ppm) by a lock mass procedure (see Table S1, SI). The product ion experiments upon CID to trigger the decarboxylation were performed in the linear ion trap (LTQ) part of the LTQ-Orbitrap XL instrument by CID with the He bath gas present ($P = 2 \times 10^{-5}$ Torr; 2.7 mbar). The product ions were analyzed in the orbitrap (Figures S19-S24, SI). Typical (+)ESI-MS conditions: Flow rate: 5 μ L min⁻¹; Capillary voltage: 3.20 kV; Sheath gas: 4.99 [arb. units]; Aux gas: 2.00 [arb. units]; resolution: 30000 fwhm.⁹ Additional MS-data and spectra are presented in the SI.

4.3. Infrared Ion Spectroscopy

A modified 3D quadrupole ion trap mass spectrometer (Bruker, Amazon Speed) was used for the infrared (IR) ion spectroscopy study, which has been described in detail elsewhere.²¹ The 3D quadrupole ion trap was operated at ambient temperature (~ 320 K) with He buffer gas at a pressure of $\sim 10^{-3}$ mbar.²¹ Wave-

length tunable laser radiation was generated by the Free Electron Laser for Infrared eXperiments (FELIX) in the 600–1900 cm^{-1} range for all IRMPD spectroscopy experiments.²¹ Additionally, a pulsed OPO (LaserVision, USA) source was used to cover the 3200–3800 cm^{-1} range.⁸ Both lasers operate with a repetition frequency of 10 Hz. The FEL pulse energies were approximately 50–100 mJ per 5 μs long macropulse and OPO delivered 10–20 mJ per 5 ns long pulse. The full width at half-maximum bandwidth of the FEL is approximately 0.4% of the central wavelength and 3 cm^{-1} for the OPO. Gas-phase precursor ions for IR ion spectroscopy were generated by electrospray ionization in positive ion mode from 0.5 μM solutions of analyte in CH_3CN at a flow rate of 120 $\mu\text{L h}^{-1}$. Ions were irradiated with 1–10 laser pulses in order to observe IR frequency dependent photodissociation. Unimolecular dissociation results from the absorption of multiple IR photons (IRMPD) with effective intramolecular vibrational redistribution (IVR) of the excitation energy leading to non-coherent photo activation until the threshold for dissociation is reached.^{8, 20–22} The IR photodissociation yield ($\Sigma I_{\text{fragment ions}}/\Sigma I_{\text{all ions}}$) is obtained from monitoring the depletion of the precursor ion signal and the increase of intensity of photo dissociation product ion signals. An IR spectrum is obtained by plotting $-\ln(1-\text{yield})$ as a function of IR frequency.³³ The IR intensity was linearly corrected for the frequency-dependent variations in laser pulse energy.³³ A grating spectrometer (wavemeter) was used to calibrate the absolute frequency of the FEL (OPO).

4.4 Kinetics

The kinetic studies were conducted at IR frequencies where the carbenes absorb (ν C–OH stretching mode, around 1300 cm^{-1}) and the aldehydes are transparent, and *vice versa* (ν_{as} C=O stretching mode, around 1740 cm^{-1}). Before the actual kinetic measurement, two parameters have to be determined. The first one is the laser pulse energy at 1300 cm^{-1} for which the aldehydes do not dissociate. The second parameter is the number of pulses needed to dissociate *all* carbene or aldehyde ions. Both parameters can be obtained from an isomer population analysis (IPA)³³ where the precursor intensity is measured as function of the number of laser pulses (for various laser pulse energies). For the kinetic measurements described here, 5 pulses (0.5 s of irradiation) were used to dissociate all carbene or aldehydes. A kinetics graph is obtained by plotting the dissociation yield as function of the time delay (0–20 s) between formation of the precursor ion and laser irradiation. At each time step, 3–5 mass spectra were averaged. Each kinetic measurement was performed 2–5 times. All experiments (IRIS, IPA, kinetics) are fully automated by controlling and storing all MS, MS/MS, and laser parameters in Bruker Compass software using an XML scripting interface within an in-house designed LabView program.³³

4.5 Computations

4.5.1 Density Functional Theory Calculations

Density functional theory (DFT) calculations were performed using Gaussian09, version E.01.³⁵ Gaussian was compiled with Gaussian-supplied versions of BLAS and ATLAS.³⁶ The B3LYP³⁷ functional was used throughout this study with the D3-BJ correction³⁸ to account for dispersion interactions,

whereby it is noted that in this case the correction did not significantly affect the results in comparison to the bare B3LYP functional. The cc-pVTZ basis set³⁹ was used throughout with the ultrafine setting for the integrals. This computational procedure is an improvement on the procedure from our earlier work, which already gave a good correlation with experiments^{20c, 40, 41} and is consistent with the approach taken in Ref. 8. All calculations performed on these systems were done *in vacuo*. Minima were confirmed through the absence of any imaginary frequencies. Intrinsic reaction coordinate (IRC) calculations were performed with the calculation of frequencies at every step of the profile to check the validity of the transition states, which were identified by a single imaginary frequency. CCSD(T)-F12b⁴² calculations were carried out with the MOLPRO package of ab initio programs,⁴³ using the cc-pVDZ basis set⁴⁴ along with matching auxiliary fitting bases.⁴⁵ The geminal Slater exponent was set to 1.0 a_0^{-1} . The overlay between X-ray and calculated structure in Figure S50 was generated using ROCS, part of the OpenEye Toolkit.⁴⁶

All calculations were performed as singlets in a restricted formalism, except for three calculations on relevant triplet states, which were performed in an unrestricted formalism. The electronic energies of all triplet states were found to be at least 135 kJ mol^{-1} above the 7- H_{5r} singlet state. Specifically, the computations yielded the following values: 7- H_{5r} triplet: 135.3 kJ mol^{-1} , 7- H_{7r} triplet: 185.3 kJ mol^{-1} , 7- H_{6c} triplet: 181.3 kJ mol^{-1} .

4.5.2 Rate determinations

Full details of the SCTST method can be found in Refs. 32 and 47. Calculations were performed using the pySCTST code, which was adapted to take into account local variations of the python libraries.³¹ The underpinning theoretical methods used in the rate calculations were identical to those used in the calculation of the energy profiles, *i.e.* density functional theory (DFT) calculations were performed using Gaussian09, version E.01.³⁶ The B3LYP³⁷ functional was used throughout this study including the D3-BJ correction³⁹ and the cc-pVTZ basis set⁴⁰ with the ultrafine setting for the integrals.

ASSOCIATED CONTENT

Supporting Information

The Supporting Information is available free of charge on the ACS Publications website at DOI:XXXXXXXX.

Experimental details of the synthesis of the carbene precursors and reference aldehydes; ESI-MS; ESI-MS², and IR ion spectra, Data analysis of the tautomer selective kinetics measurements, Energy profiles of carbene formation and isomerization to the respective aldehyde and enols of the analytes of interest; Cartesian coordinates and energies of all calculated structures, Additional Figures and Tables (PDF)

X-ray data of 5-(Trimethylammonio)-2-oxopentanoate (**6**) (CIF), of (N-Methyl-4-quinuclidinio)glyoxylate hydrate (**10**· H_2O) (CIF), and of (N-Methyl-4-quinuclidinio)carbaldehyde (**12**) (CIF).

AUTHOR INFORMATION

Corresponding Authors

* mthias.schaefer@uni-koeln.de, j.oomens@science.ru.nl
a.meijer@sheffield.ac.uk, berkessel@uni-koeln.de

ACKNOWLEDGMENT

We gratefully acknowledge Radboud University and the Nederlandse Organisatie voor Wetenschappelijk Onderzoek (NWO), for support of the FELIX Laboratory. Funding from the Deutsche Forschungsgemeinschaft (DFG, Grant No. SCHA 871/10-1) as well as (DFG, Grant No. BE 998/16-1) is gratefully acknowledged. The research leading to these results has received funding from LASERLAB-EUROPE (Grant Agreement No. 871124, European Union's Horizon 2020 research and innovation program). We wish to thank Dr. J. Grant Hill of the University of Sheffield for his help in running the CCSD(T) calculations and Dr. Timothy Burd for his help in running the pySCTST code. A license for the OpenEye tools, obtained via the free academic licensing program, is gratefully acknowledged.

ABBREVIATIONS

CID: Collision Induced Dissociation
 IPA: isomer population analysis
 IRC: Intrinsic Reaction Coordinate
 IRIS: Infrared Ion Spectroscopy
 IRMPD: Infrared Multiple-Photon Dissociation
 DCM: Dichloromethane
 ESI: Electrospray
 DFT: Density Functional Theory
 FEL: Free Electron Laser
 FELIX: Free Electron Laser for Infrared eXperiments
 HVFP: High-Vacuum Flash Pyrolysis
 IVR: Intramolecular Vibrational Redistribution
 KIE: Kinetic Isotope Effect
 LTQ: Linear Ion Trap
 OPO: Optical Parametric Oscillator
 QIT: Quadrupole Ion Trap
 QMHT: Quantum-Mechanical Hydrogen Tunneling
 SCTST: Semi-classical Transition State Theory

REFERENCES

(1) (a) Bell, R. P. *The Tunnel Effect in Chemistry*, Springer, New York, NY, USA, 1980. (b) Meisner, J.; Kästner, J. Atom Tunneling in Chemistry, *Angew. Chem. Int. Ed.*, **2016**, *55*, 5400-5413. (c) McMahon, R.J. Chemical Reactions Involving Quantum Tunneling, *Science* **2003**, *299*, 833-834. (d) Kästner, J. Path Length Determines the Tunneling Decay of Substituted Carbenes, *Chem. Eur. J.* **2013**, *19*, 8207-8212.
 (2) (a) Borden, W. T. Reactions that involve tunneling by carbon and the role that calculations have played in their study, *WIREs Comput. Mol. Sci.* **2016**, *6*, 20-46. (b) Kästner, J. Theory and simulation of atom tunneling in chemical reactions, *WIREs Comp. Mol. Sci.* **2014**, *4*, 158-168.
 (3) Schreiner, P.R.; Reisenauer, H.P.; Ley, D.; Gerbig, D.; Wu, C.-H.; Allen, W.D. Methylhydroxycarbene: Tunneling Control of a Chemical Reaction, *Science*, **2011**, *332*, 1300-1303.
 (4) (a) Schreiner, P. R. Tunneling Control of Chemical Reactions: The Third Reactivity Paradigm, *J. Am. Chem. Soc.* **2017**, *139*, 15276-15283. (b) Schreiner, P. R. Quantum Mechanical Tunneling Is Essential to Understanding Chemical Reactivity, *Trends in Chemistry*, **2020**, *2*, 980-989. (c) Ley, D.; Dennis Gerbig, D.; Schreiner, P. R. Tunneling control of chemical reactions: C-H insertion versus H-tunneling in tert-butylhydroxycarbene, *Chem. Sci.*, **2013**, *4*, 677-684.
 (5) Schleif, T.; Mieres-Perez, J.; Henkel, S.; Ertelt, M.; Borden, W. T.; Sander, W. The Cope Rearrangement of 1,5 Dimethylsemibullvalene-

2(4)-d1: Experimental Evidence for Heavy-Atom Tunneling, *Angew. Chem. Int. Ed.* **2017**, *56*, 10746-10749.

(6) (a) Zuev, P. S.; Sheridan, R. S.; Albu, T. V.; Truhlar, D. G.; Hrovat, D. A.; Borden, W. T. Carbon Tunneling from a Single Quantum State, *Science* **2003**, *299*, 867-870. (b) Zhang, X.; Hrovat, D.A.; Borden, W.T. Calculations Predict That Carbon Tunneling Allows the Degenerate Cope Rearrangement of Semibullvalene to Occur Rapidly at Cryogenic Temperatures, *Org. Lett.*, **2010**, *12*, 2798-2801.

(7) Schleif, T.; Merini, M. P.; Henkel, S.; Sander, W. Solvation Effects on Quantum Tunneling Reactions, *Acc. Chem. Res.* **2022**, *55*, 2180-2190.

(8) Schäfer, M.; Peckelsen, K.; Paul, M.; Martens, J.; Oomens, J.; Berden, G.; Berkessel, A.; Meijer, A. J. H. M. Hydrogen Tunneling above Room Temperature Evidenced by Infrared Ion Spectroscopy, *J. Am. Chem. Soc.*, **2017**, *139*, 5779-5786.

(9) Paul, M.; Peckelsen, K.; Thomulka, T.; Neudörfl, J.; Martens, J.; Berden, G.; Oomens, J.; Berkessel, A.; Meijer, A.J.H.M.; Schäfer, M. Hydrogen tunneling avoided: enol-formation from a charge-tagged phenyl pyruvic acid derivative evidenced by tandem-MS, IR ion spectroscopy and theory, *Phys. Chem. Chem. Phys.*, **2019**, *21*, 16591-16600.

(10) Burd, T.A. H.; Shan, X.; Clary, D. C. Hydrogen tunnelling in the rearrangements of carbenes: the role of dynamical calculations, *Phys. Chem. Chem. Phys.*, **2020**, *22*, 962-965.

(11) (a) Schreiner, P. R.; Reisenauer, H. P.; Pickard IV, F. C.; Simonett, A.C.; Allen, W. D.; Mátyus, E.; Császár, A. G. Capture of hydroxymethylene and its fast disappearance through tunnelling, *Nature* **2008**, *453*, 906-909. (b) Bucher, G. Hydroxycarbene: Watching a Molecular Mole at Work, *Angew. Chem. Int. Ed.* **2008**, *47*, 6957-6958.

(12) Eckhardt, A. K.; Gerbig, D.; Schreiner, P. R. Heavy Atom Secondary Kinetic Isotope Effect on H-Tunneling, *J. Phys. Chem. A* **2018**, *122*, 1488-1495.

(13) Gerbig, D.; Reisenauer, H.P.; Wu, C.H.; Ley, D.; Allen, W.D.; Schreiner, P. R. Phenylhydroxycarbene, *J. Am. Chem. Soc.* **2010**, *132*, 7273-7275.

(14) Ley, D.; Gerbig, D.; Wagner, J.P.; Reisenauer, H.P.; Schreiner, P.R. Cyclopropylhydroxycarbene, *J. Am. Chem. Soc.* **2011**, *133*, 13614-13621.

(15) Eckhardt, A.K.; Erb, F. R.; Schreiner, P.R. Conformer-specific [1,2] H-tunnelling in captodatively-stabilized cyanohydroxycarbene (NC-C-OH), *Chem. Sci.*, **2019**, *10*, 802-808.

(16) Eckhardt, A.K.; Schreiner, P.R. Spectroscopic Evidence for Aminomethylene (H-C-NH₂) -The Simplest Amino Carbene, *Angew. Chem. Int. Ed.* **2018**, *57*, 5248-5252.

(17) Oehler, E.; Schmidt, U. Hydroxylsubstituierte Cyclodipeptide durch Ringschluß von Pyruvoylaminosiiureamiden, *Chem. Ber.* **1975**, *108*, 2907-2916.

(18) Grob, C. A.; Brenneisen, P. Die Synthese von 4-Brom- und 4-Hydroxy-chinuclidin. Untersuchungen in der Chinuclidin-Reihe, 6. Mitteilung, *Helv. Chim. Acta* **1958**, *41*, 1184-1190.

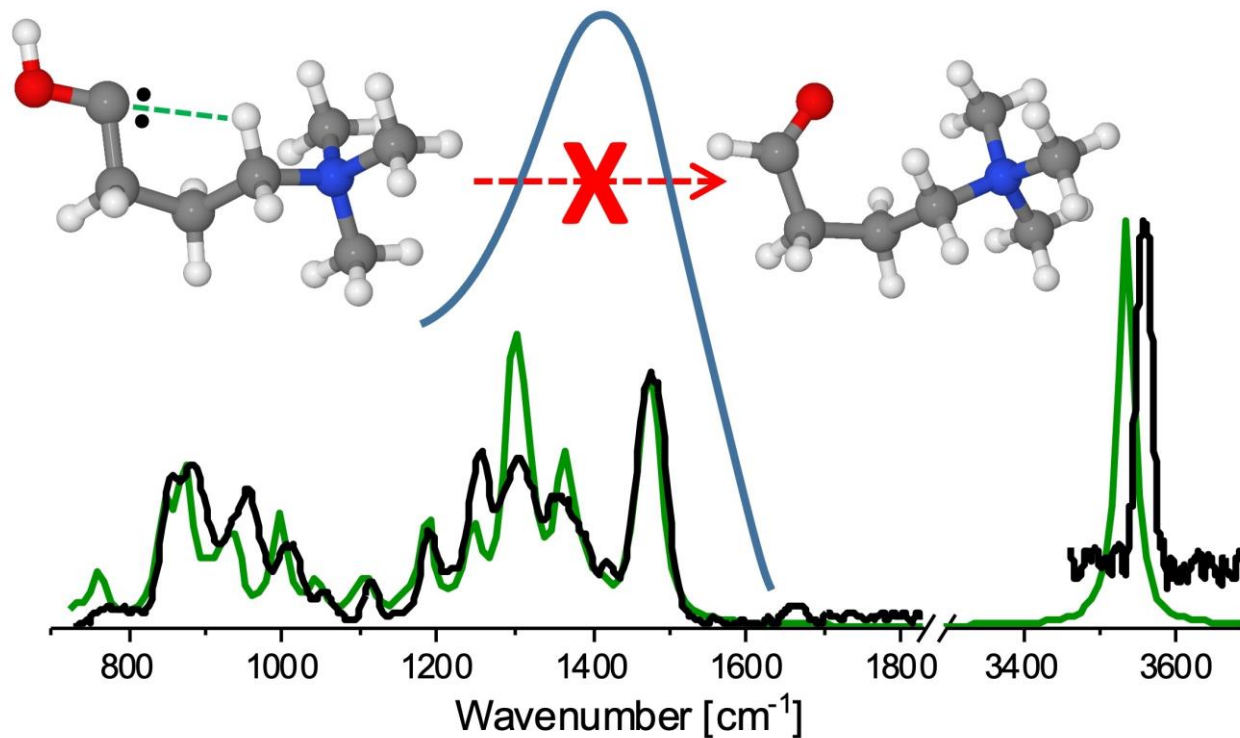
(19) Dumele, O.; Schreiber, B.; Warzok, U.; Trapp, N.; Schalley, C. A.; Diederich, F. Halogen-Bonded Supramolecular Capsules in the Solid State, in Solution, and in the Gas Phase, *Angew. Chem. Int. Ed.* **2017**, *56*, 1152-1157.

(20) (a) Peckelsen, K.; Martens, J.; Czypiel, L.; Oomens, J.; Berden, G.; Gründemann, D.; Meijer, A.J.H.M.; Schäfer, M. Ergothioneine and related histidine derivatives in the gas phase: tautomer structures determined by IRMPD spectroscopy and theory, *Phys. Chem. Chem. Phys.* **2017**, *19*, 23362-23372. (b) Peckelsen, K.; Martens, J.; Berden, G.; Oomens, J.; Dunbar, R.C.; Meijer, A.J.H.M.; Schäfer, M. Gas-phase complexes of Ni²⁺ and Ca²⁺ with deprotonated histidylhistidine (HisHis): A model case for polyhistidyl-metal binding motifs, *J. Mol. Spec.* **2017**, *332*, 38-44. (c) Holland, M.C.; Berden, G.; Oomens, J.; Meijer, A.J.H.M.; Schäfer, M.; Gilmour, R. Infrared Multiphoton Dissociation Spectroscopic Analysis of Noncovalent Interactions in Organocatalysis, *Eur. J. Org. Chem.* **2014**, 5675-5680. (d) Brückmann, L.; Tyrra, W.; Mathur, S.; Berden, G.; Oomens, J.; Meijer, A.J.H.M.; Schäfer, M. Examination of the Coordination Sphere of AlIII in Trifluoromethyl-Heteroarylalkenolato Complex Ions by Gas-Phase

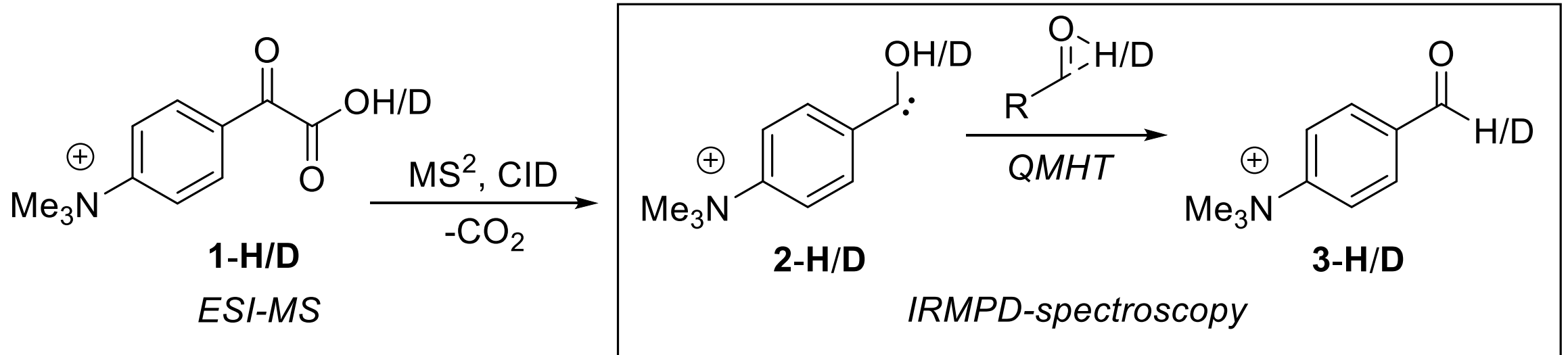
- IRMPD Spectroscopy and Computational Modelling, *ChemPhysChem*, **2012**, *13*, 2037-2045. (e) Stevenson, B.C.; Peckelsen, K.; Martens, J.; Berden, G.; Oomens, J.; Schäfer, M.; Armentrout, P.B. An investigation of inter-ligand coordination and flexibility: IRMPD spectroscopic and theoretical evaluation of calcium and nickel histidine dimers, *J. Mol. Spec.* **2021**, *381*, 111532.
- (21) (a) Martens, J.; Grzetic, J.; Berden, G.; Oomens, J. Structural identification of electron transfer dissociation products in mass spectrometry using infrared ion spectroscopy, *J. Nat. Commun.* **2016**, *7*, 11754. (b) Martens, J.; Berden, G.; Gebhardt, C.R.; Oomens, J., Infrared ion spectroscopy in a modified quadrupole ion trap mass spectrometer at the FELIX free electron laser laboratory, *Rev. Sci. Instrum.* **2016**, *87*, 103108.
- (22) (a) Polfer, N. C. Infrared multiple photon dissociation spectroscopy of trapped ions, *Chem. Soc. Rev.* **2011**, *40*, 2211-2221. (b) Polfer, N. C.; Oomens, J. Vibrational spectroscopy of bare and solvated ionic complexes of biological relevance, *Mass Spectrom. Rev.* **2009**, *28*, 468-494. (c) Roithova, J. Characterization of reaction intermediates by ion spectroscopy, *J. Chem. Soc. Rev.* **2012**, *41*, 547-559. (d) A.M. Rijs, J. Oomens, IR Spectroscopic Techniques to Study Isolated Biomolecules in Gas-Phase IR Spectroscopy and Structure of Biological Molecules, Book Series: Topics in Current Chemistry-Series, Springer **2015**, *364*, 1-42. (e) Jasikova, L.; Roithova, J. Infrared Multiphoton Dissociation Spectroscopy with Free-Electron Lasers: On the Road from Small Molecules to Biomolecules, *Chem. Eur. J.* **2018**, *24*, 3374-3390. (f) Martens, J.; van Outersterp, R. E.; Vreeken, R. J.; Cuyckens, F.; Coene, K. L.M.; Engelke, U. F.; Kluijtmans, L. A.J.; Wevers, R. A.; Buydens, L. M.C.; Redlich, B.; Berden, G.; Oomens, J. Infrared ion spectroscopy: New opportunities for small-molecule identification in mass spectrometry - A tutorial perspective, *Anal. Chim. Acta* **2020**, *1093*, 1-15. (g) Pereverzev, A.; Roitova, J. Experimental techniques and terminology in gas-phase ion spectroscopy, *J. Mass Spectrom.* **2022**, *57*, e4826. 10.1002/jms.4826.
- (23) (a) Alkorta, I.; Rozas, I.; Elguero, J. Non-conventional hydrogen bonds, *Chem. Soc. Rev.*, **1998**, *27*, 163-170. (b) Arduengo, A. J., Gamper, S. F.; Tamm, M.; Calabrese, J. C.; Davidson, F.; Craig, H. A. A Bis(carbene)-Proton Complex: Structure of a C-H-C Hydrogen Bond, *J. Am. Chem. Soc.* **1995**, *117*, 572-573. (c) S. T. Howard, C. D. Abernethy, Intramolecular C-H...Ccarbene Hydrogen Bonds and Competing Interactions in Monoprotonated Tripodal Carbenes, *J. Comp. Chem.* **2003**, *25*, 649-659. (d) Leites, L. A.; Magdanurov, G. I.; Bukalov, S. S.; West, R. Intermolecular =C-H...C hydrogen bond in a crystalline unsaturated Arduengo-type carbene, *Mendeleev Commun.*, **2008**, *18*, 14-15. (e) Holloczki, O. Unveiling the peculiar hydrogen bonding behavior of solvated N-heterocyclic carbenes, *Phys. Chem. Chem. Phys.*, **2016**, *18*, 126-140. (f) Alkorta, I.; Elguero, J. Carbenes and Silylenes as Hydrogen Bond Acceptors, *J. Phys. Chem.* **1996**, *100*, 19367-19370.
- (24) (a) Hadel, L. M.; Platz, M. S.; Scaiano, J. C.; Study of Hydrogen Atom Abstraction Reactions of Triplet Diphenylcarbene in Solution, *J. Am. Chem. Soc.* **1984**, *106*, 283-287. (b) Doering W. von E.; Buttery, R.G.; Laughlin, R.G.; Chaudhuri, N.; Indiscriminate Reaction of Methylene with the Carbon-Hydrogen Bond, *J. Am. Chem. Soc.* **1956**, *78*, 3224.
- (25) (a) Cowan, J.A.; Clyburne, J. A. C.; Davidson, M. G.; Harris, R. L. W.; Howard, J. A. K.; Küpper, P.; Leech, M. A.; Richards, S. P. On the Interaction between N-Heterocyclic Carbenes and Organic Acids: Structural Authentication of the First N-H...C Hydrogen Bond and Remarkably Short C-H...O Interactions, *Angew. Chem. Int. Ed.* **2002**, *41*, 1432-1433. (b) Raut, A. H.; Karir, G.; Viswanathan, K. S. Matrix Isolation Infrared and Ab Initio Study of the Interaction of N-Heterocyclic Carbene with Water and Methanol: A Case Study of a Strong Hydrogen Bond, *J. Phys. Chem. A* **2016**, *120*, 9390-9400. (c) Knorr, J.; Sokkar, P.; Schott, S.; Costa, P.; Thiel, W.; Sander, W.; Sanchez-Garcia, E.; Nuernberger, P. Competitive solvent-molecule interactions govern primary processes of diphenylcarbene in solvent mixtures, *Nat. Commun.* **2016**, *7*, 12968. (d) Del Bene, J. E.; Alkorta, I.; Elguero, J. Hydrogen-bonded complexes with carbenes as electron-pair donors, *Chem. Phys. Lett.* **2017**, *675*, 46-50. (e) Richter, G.; Mendez-Vega, E.; Sander, W. Singlet Halophenylcarbenes as Strong Hydrogen-Bond Acceptors, *J. Phys. Chem. A* **2016**, *120*, 3524-3532. (f) Standard, J. M. Effects of Solvation and Hydrogen Bond Formation on Singlet and Triplet Alkyl or Aryl Carbenes, *J. Phys. Chem. A* **2017**, *121*, 381-393. (g) Costa, P.; Sander, W. Hydrogen Bonding Switches the Spin State of Diphenylcarbene from Triplet to Singlet, *Angew. Chem. Int. Ed.* **2014**, *53*, 5122-5125.
- (26) Pettersson, M.; Macoas, E. M. S.; Khriachtchev, L.; Lundell, J.; Fausto, R.; Räsänen, M. Cis→trans conversion of formic acid by dissipative tunneling in solid rare gases: Influence of environment on the tunneling rate, *J. Chem. Phys.* **2002**, *117*, 9095-9098.
- (27) (a) Schwartz, J.; Senko, M. W.; Syka, J. E. P. A two-dimensional quadrupole ion trap mass spectrometer, *J. Am. Soc. Mass Spectrom.* **2002**, *13*, 659-669. (b) Stafford Jr., G.C.; Kelley, P.E.; Syka, J.E.P.; Reynolds, W.E.; Todd, J.F.J. Recent Improvements in and Analytical Applications of Advanced Ion Trap Technology, *Int. J. Mass Spectrom. Ion Proc.*, **1984**, *60*, 85-98.
- (28) (a) Heard, D. E. Rapid Acceleration of Hydrogen Atom Abstraction Reactions of OH at Very Low Temperatures through Weakly Bound Complexes and Tunneling, *Acc. Chem. Res.* **2018**, *51*, 2620-2627. (b) Miyazaki T. (Ed.) *Springer Series on Atomic, Optical, and Plasma Physics, Vol. 36, Miyazaki, T., Atom Tunneling Phenomena in Physics, Chemistry and Biology, Springer, Berlin, Heidelberg, 2004.*
- (29) Miller, W. H. Semi-classical theory for non-separable systems: Construction of "good" action-angle variables for reaction rate constants, *Faraday Discuss. Chem. Soc.* **1977**, *62*, 40-44.
- (30) Miller, W. H.; Hernandez, R.; Handy, N. C.; Jayatilaka, D.; Willetts, A. Ab initio calculation of anharmonic constants for a transition state, with application to semi-classical transition state tunneling probabilities, *Chem. Phys. Lett.* **1990**, *172*, 62-68.
- (31) Burd, T.A.H. pySCTST, <https://bitbucket.com/timothy-burd/pysctst>, 2019. [last accessed: 16 Dec 2022]
- (32)(a) Benkovic, S. J.; Hammes-Schiffer, S. Enzyme Motions Inside and Out, *Science*, **2006**, *312*, 208-209. (b) Layfield, J. P.; Hammes-Schiffer, S. Hydrogen Tunneling in Enzymes and Biomimetic Models, *Chem. Rev.* **2014**, *114*, 3466-3494. (c) Trakhtenberg, L. I.; Nadochenko, V. A. Tunneling Proton Transfer in Biological Systems. Role of Temperature and Pressure, *Russ. J. Phys. Chem. A* **2012**, *86*, 1399-1406. (d) Johannissen, L. O.; Hay, S.; Scrutton, N. S. Nuclear quantum tunnelling in enzymatic reactions - an enzymologist's perspective, *Phys. Chem. Chem. Phys.*, **2015**, *17*, 30775-30782. (d) Vardi-Kilshain, A.; Nitoker, N.; Major, D. T. Nuclear quantum effects and kinetic isotope effects in enzyme reactions, *Arch. Biochem. Biophys.* **2015**, *582*, 18-27.
- (33) Berden, G.; Derksen, M.; Houthuijs, K.J.; Martens, J.; Oomens, J. An automatic variable laser attenuator for IRMPD spectroscopy and analysis of power-dependence in fragmentation spectra, *Int. J. Mass Spectrom.* **2019**, *443*, 1-8.
- (34) van Geenen, F. A. M. G.; Kranenburg, R. F.; van Asten, A.C.; Martens, J.; Oomens, J.; Berden, G. Isomer-Specific Two-Color Double-Resonance IR²MS³ Ion Spectroscopy Using a Single Laser: Application in the Identification of Novel Psychoactive Substances, *Anal. Chem.* **2021**, *93*, 2687-2693.
- (35) Frisch, M. J.; Trucks, G. W.; Schlegel, H. B.; Scuseria, G. E.; Robb, M. A.; Cheeseman, J. R.; Scalmani, G.; Barone, V.; Mennucci, B.; Petersson, G. A.; Nakatsuji, H.; Caricato, M.; Li, X.; Hratchian, H. P.; Izmaylov, A. F.; Bloino, J.; Zheng, G.; Sonnenberg, J. L.; Hada, M.; Ehara, M.; Toyota, K.; Fukuda, R.; Hasegawa, J.; Ishida, M.; Nakajima, T.; Honda, Y.; Kitao, O.; Nakai, H.; Vreven, T.; Montgomery, J. A., Jr.; Peralta, J. E.; Ogliaro, F.; Bearpark, M.; Heyd, J. J.; Brothers, E.; Kudin, K. N.; Staroverov, V. N.; Kobayashi, R.; Normand, J.; Raghavachari, K.; Rendell, A.; Burant, J. C.; Iyengar, S. S.; Tomasi, J.; Cossi, M.; Rega, N.; Millam, J. M.; Klene, M.; Knox, J. E.; Cross, J. B.; Bakken, V.; Adamo, C.; Jaramillo, J.; Gomperts, R.; Stratmann, R. E.; Yazyev, O.; Austin, A. J.; Cammi, R.; Pomelli, C.; Ochterski, J. W.; Martin, R. L.; Morokuma, K.; Zakrzewski, V. G.; Voth, G. A.; Salvador, P.; Dannenberg, J. J.; Dapprich, S.; Daniels, A. D.; Farkas, Ö.; Foresman, J. B.; Ortiz, J. V.; Cioslowski, J.; Fox, D. J. Gaussian 09, Revision E.01, Gaussian, Inc.: Wallingford, CT, **2009**.

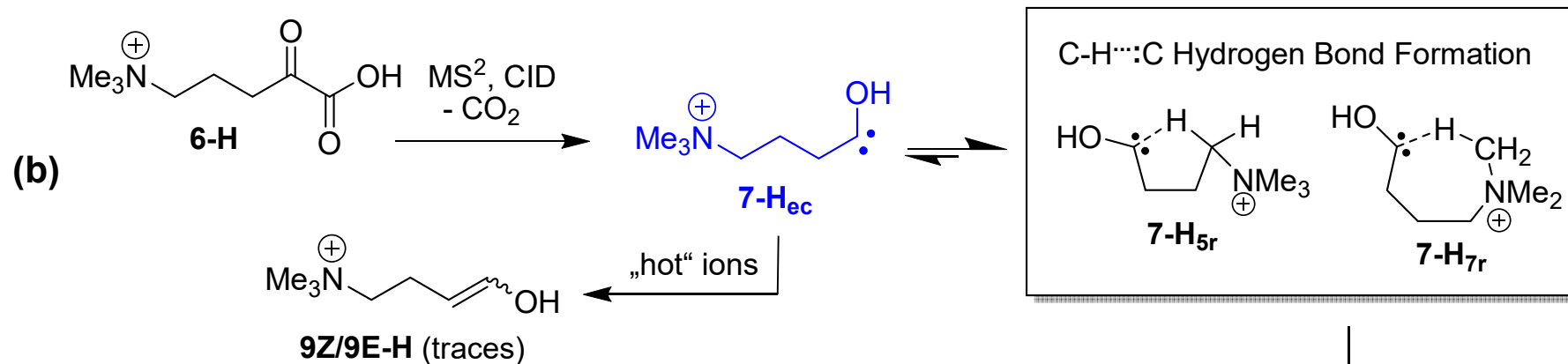
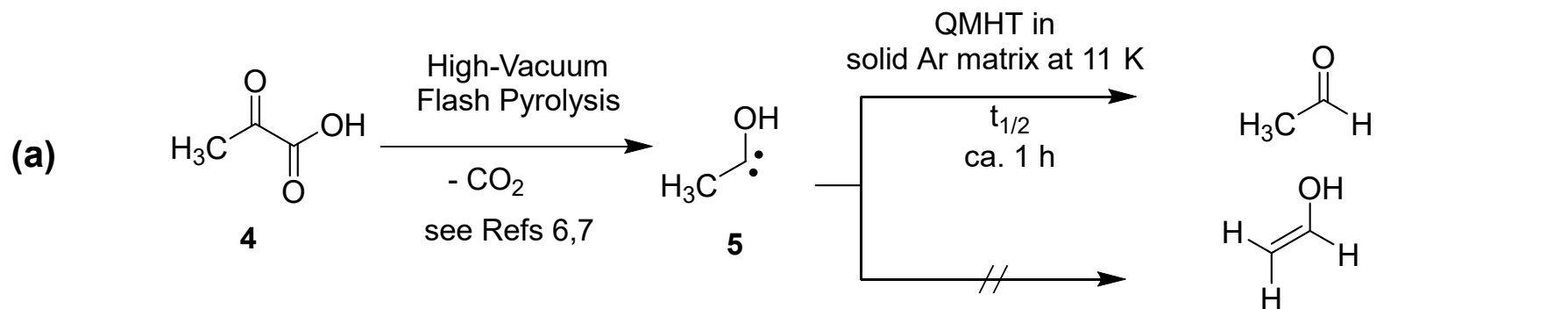
- (36) (a) Whaley, R. C.; Petitet, A. Minimizing development and maintenance costs in supporting persistently optimized BLAS, *Software Pract. Exp.* **2005**, *35*, 101-121. (b) Whaley, R. C.; Petitet, A.; Dongarra, J. J. Automated empirical optimizations of software and the ATLAS project, *Parallel Comput.* **2001**, *27*, 3-35.
- (37) Becke, A. D. Density-Functional Thermochemistry. III. The Role of Exact Exchange, *J. Chem. Phys.* **1993**, *98*, 5648-5652.
- (38) Grimme, S.; Ehrlich, S.; Goerigk, L. Effect of the damping function in dispersion corrected density functional theory, *J. Comput. Chem.* **2011**, *32*, 1456-1465.
- (39) Kendall, R. A.; Dunning, T. H.; Harrison, R. J. Electron affinities of the first-row atoms revisited. Systematic basis sets and wave functions, *J. Chem. Phys.* **1992**, *96*, 6796-6806.
- (40) Massah, A. R.; Dreiocker, F.; Jackson, R. F. W.; Pickup, B. T.; Oomens, J.; Meijer, A.J.H.M.; Schäfer, M. Gas-phase study of new organozinc reagents by IRMPD-spectroscopy, computational modelling and tandem-MS, *Phys. Chem. Chem. Phys.* **2011**, *13*, 13255-13267.
- (41) Ross, A.J.; Dreiocker, F.; Schäfer, M.; Oomens, J.; Meijer, A.J. H. M.; Pickup, B.T.; Jackson, R.F.W. Evidence for the Role of Tetramethylethylenediamine in Aqueous Negishi Cross-Coupling: Synthesis of Nonproteinogenic Phenylalanine Derivatives on Water, *J. Org. Chem.* **2011**, *76*, 1727-1734.
- (42) Knizia, G.; Adler, T. B.; Werner, H.-J. Simplified CCSD(T)-F12 methods: Theory and benchmarks, *J. Chem. Phys.* **2009**, *130*, 054104.
- (43) (a) Werner, H.-J.; Knowles, P. J.; Knizia, G.; Manby, F. R.; Schütz, M.; Celani, P.; Korona, T.; Lindh, R.; Mitrushenkov, A.; Rauhut, G.; Shamasundar, K. R.; Adler, T. B.; Amos, R. D.; Bernhardsson, A.; Berning, A.; Cooper, D. L.; Deegan, M. J. O.; Dobbyn, A. J.; Eckert, F.; Goll, E.; Hampel, C.; Hesselmann, A.; Hetzer, G.; Hrenar, T.; Jansen, G.; Köppl, C.; Liu, Y.; Lloyd, A. W.; Mata, R. A.; May, A. J.; McNicholas, S. J.; Meyer, W.; Mura, M. E.; Nicklass, A.; O'Neill, D. P.; Palmieri, P.; Peng, D.; Pflüger, K.; Pitzer, R.; Reiher, M.; Shiozaki, T.; Stoll, H.; Stone, A. J.; Tarroni, R.; Thorsteinsson, T.; Wang, M. MOLPRO, A Package of Ab Initio Programs, v. 2012.1; 2012. (b) Werner, H. J.; Knowles, P. J.; Knizia, G.; Manby, F. R.; Schütz, M. Molpro: a general-purpose quantum chemistry program package, *WIREs Comput. Mol. Sci.* **2012**, *2*, 242-253.
- (44) Peterson, K. A.; Adler, T. B.; Werner, H.-J. Systematically convergent basis sets for explicitly correlated wavefunctions: The atoms H, He, B-Ne, and Al-Ar, *J. Chem. Phys.* **2008**, *128*, 084102, 1-12.
- (45) (a) Weigend, F. A. A fully direct RI-HF algorithm: Implementation, optimised auxiliary basis sets, demonstration of accuracy and efficiency, *Phys. Chem. Chem. Phys.* **2002**, *4*, 4285- 4291. (b) Yousaf, K. E.; Peterson, K. A. Optimized auxiliary basis sets for explicitly correlated methods, *J. Chem. Phys.* **2008**, *129*, 184108. (c) Kritikou, S.; Hill, J. G. Auxiliary Basis Sets for Density Fitting in Explicitly Correlated Calculations: The Atoms H-Ar, *J. Chem. Theory Comput.* **2015**, *11*, 5269-5276.
- (46) (a) ROCS 3.5.1.2: OpenEye Scientific Software, Santa Fe, NM. <http://www.eyesopen.com>. [last accessed: 22 March 2023] (b) Hawkins, P.C.D.; Skillman, A.G. and Nicholls, A., Comparison of Shape-Matching and Docking as Virtual Screening Tools, *Journal of Medicinal Chemistry*, **2007**, *50*, 74-82.
- (47) Shan, X.; Burd, T. A. H.; Clary, D. C. New Developments in Semiclassical Transition-State Theory, *J. Phys. Chem. A*, **2019**, *123*, 4639-4657.

Table of Contents Graphic

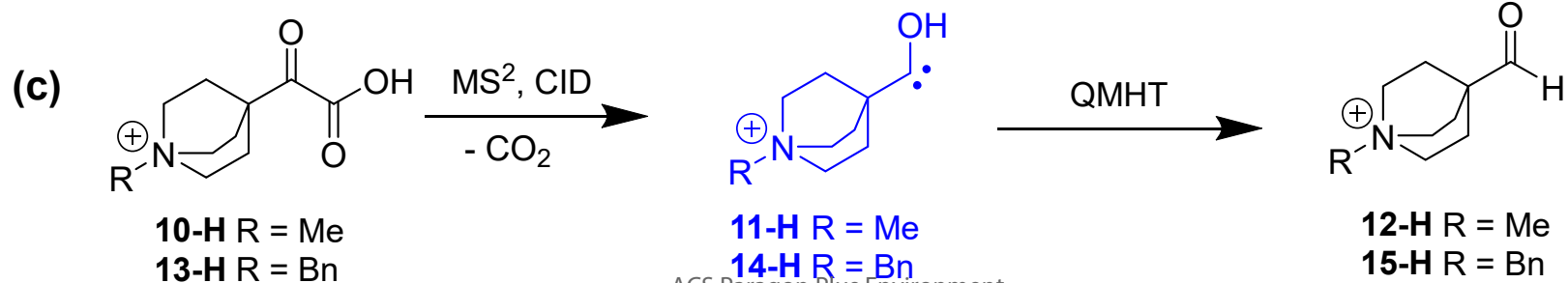
**Caption**

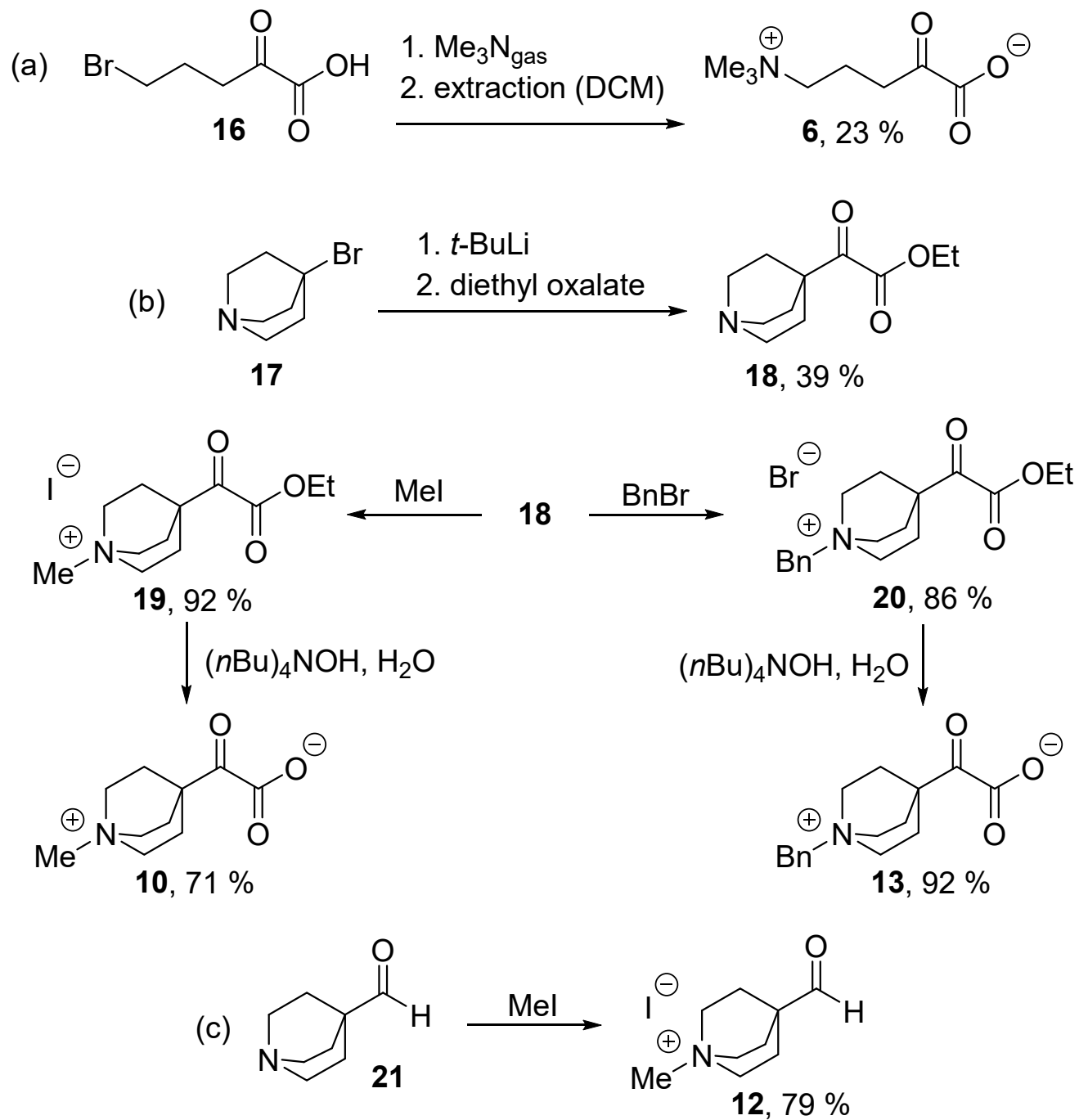
The aliphatic 3-(trimethylammonio)propylhydroxycarbene is stable in the gas phase and at room temperature performing no H-shift to *neither* aldehyde *nor* enol. As supported by IR ion spectroscopy and DFT calculations, this quantum mechanical hydrogen tunneling inhibition is due to intramolecular C...H-C bonding of the singlet carbene's free electron pair to one of the mildly acidic α -ammonio hydrogens.

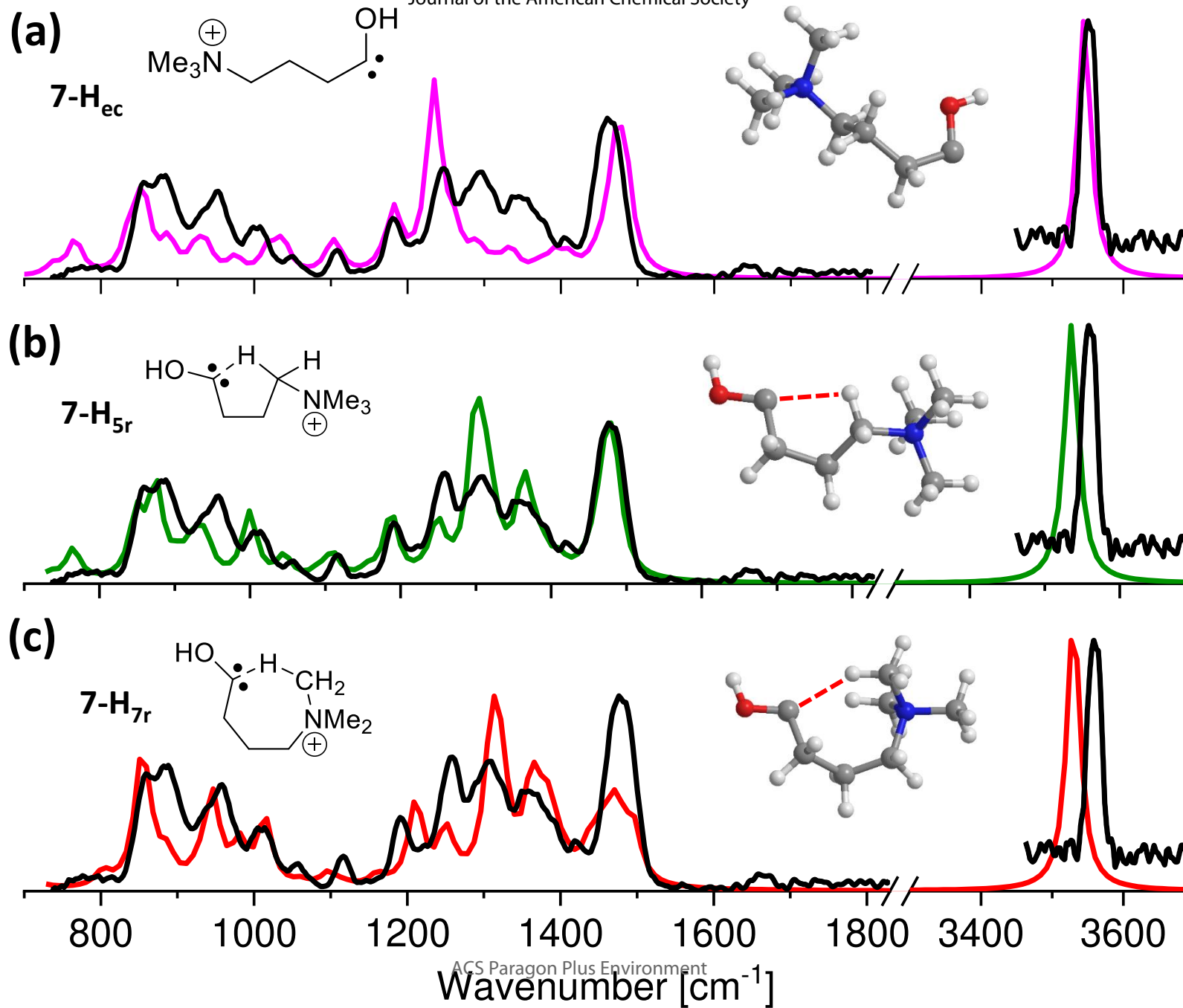


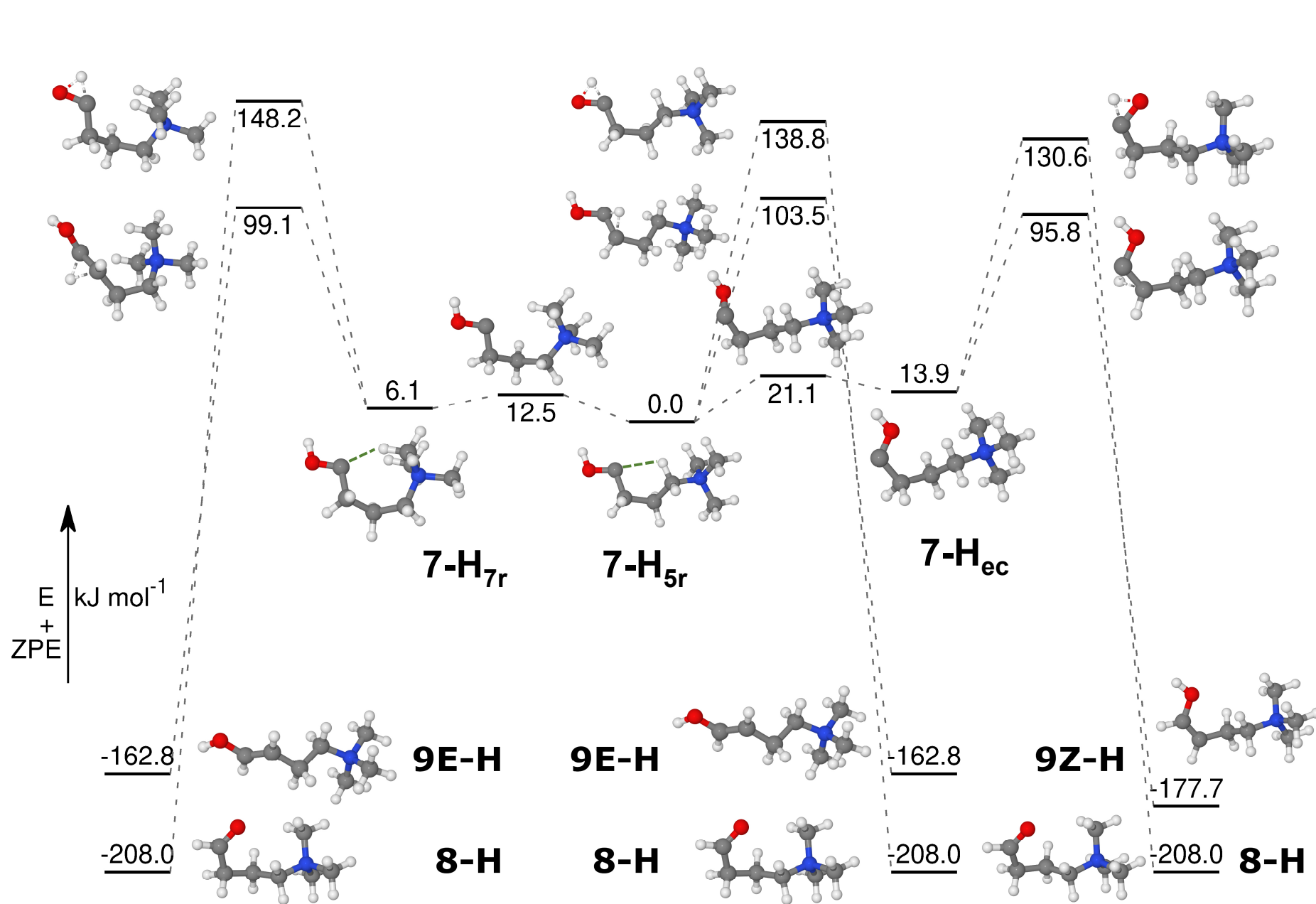


This Study:
Tandem-MS & IR Ion Spectroscopy in the Gas Phase,
at 320-350 K in a Quadrupole Ion Trap

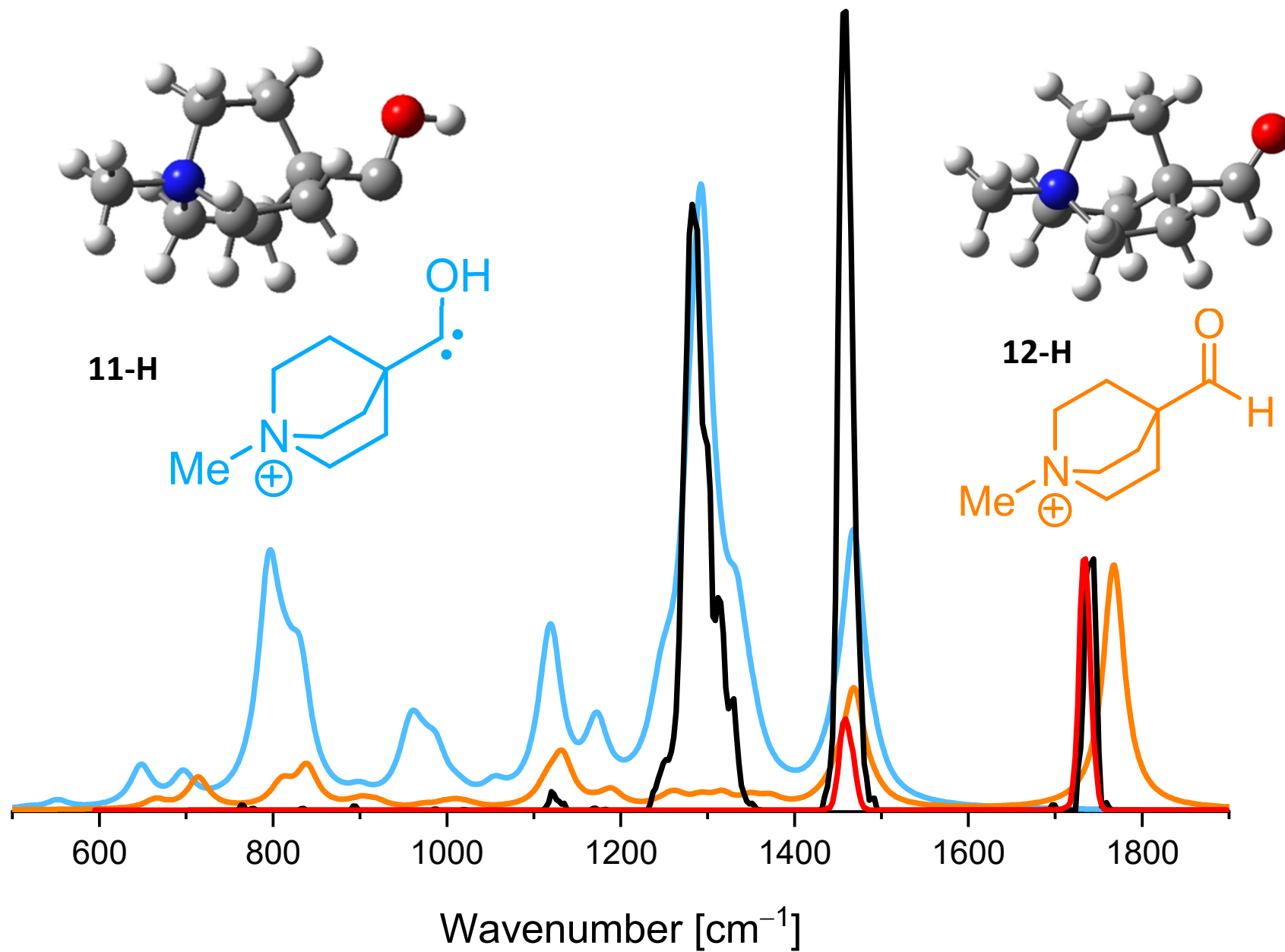




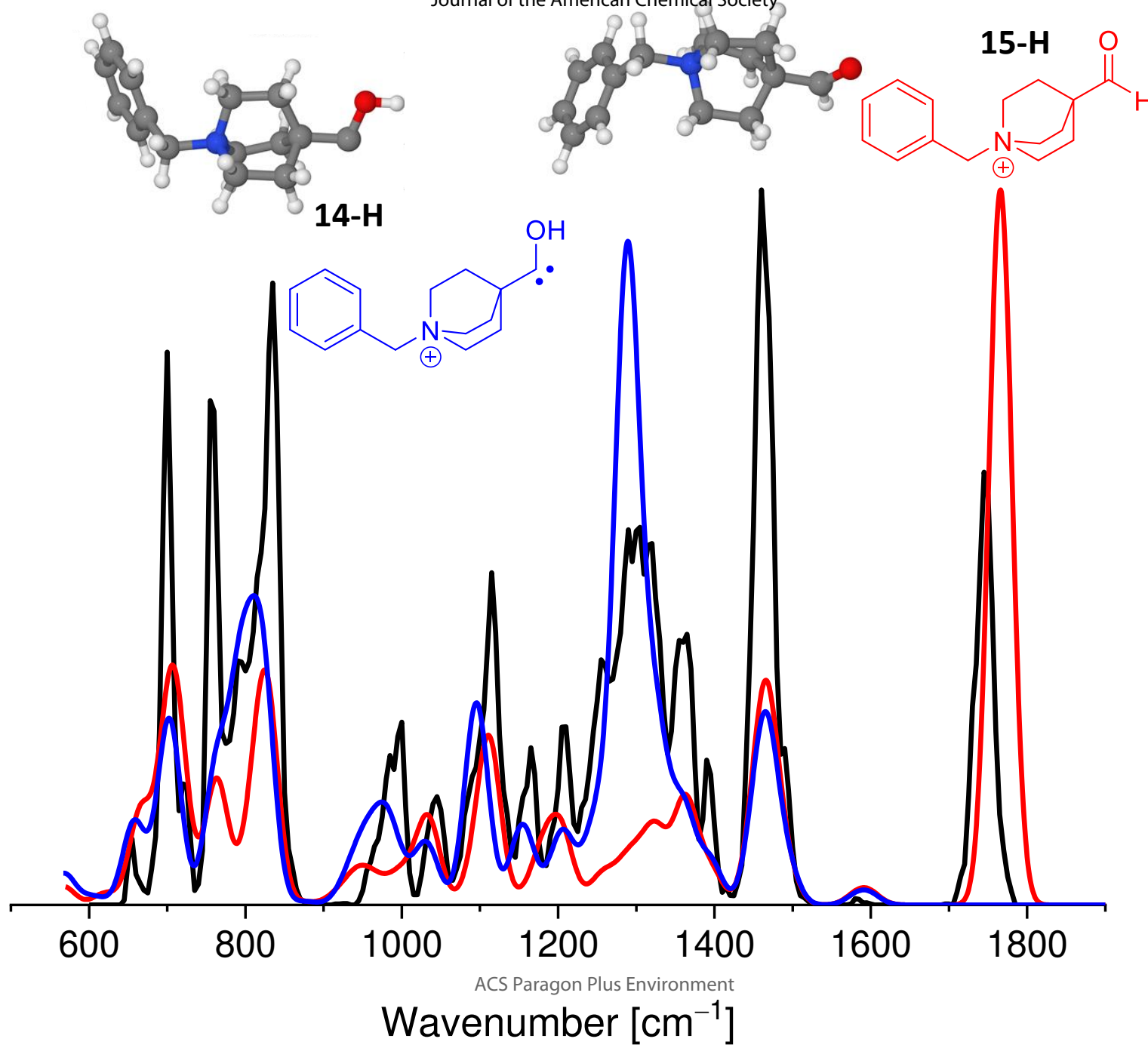


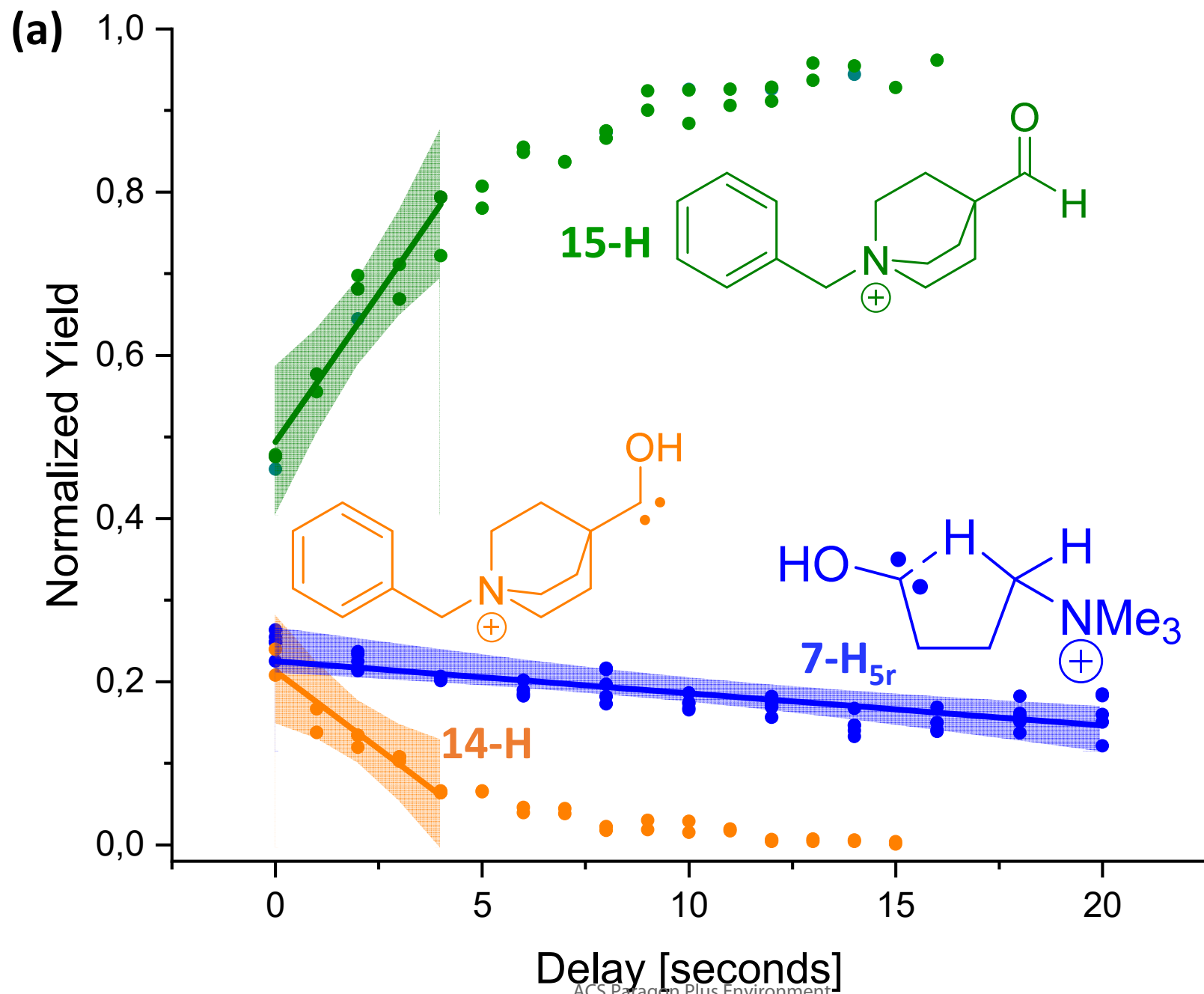


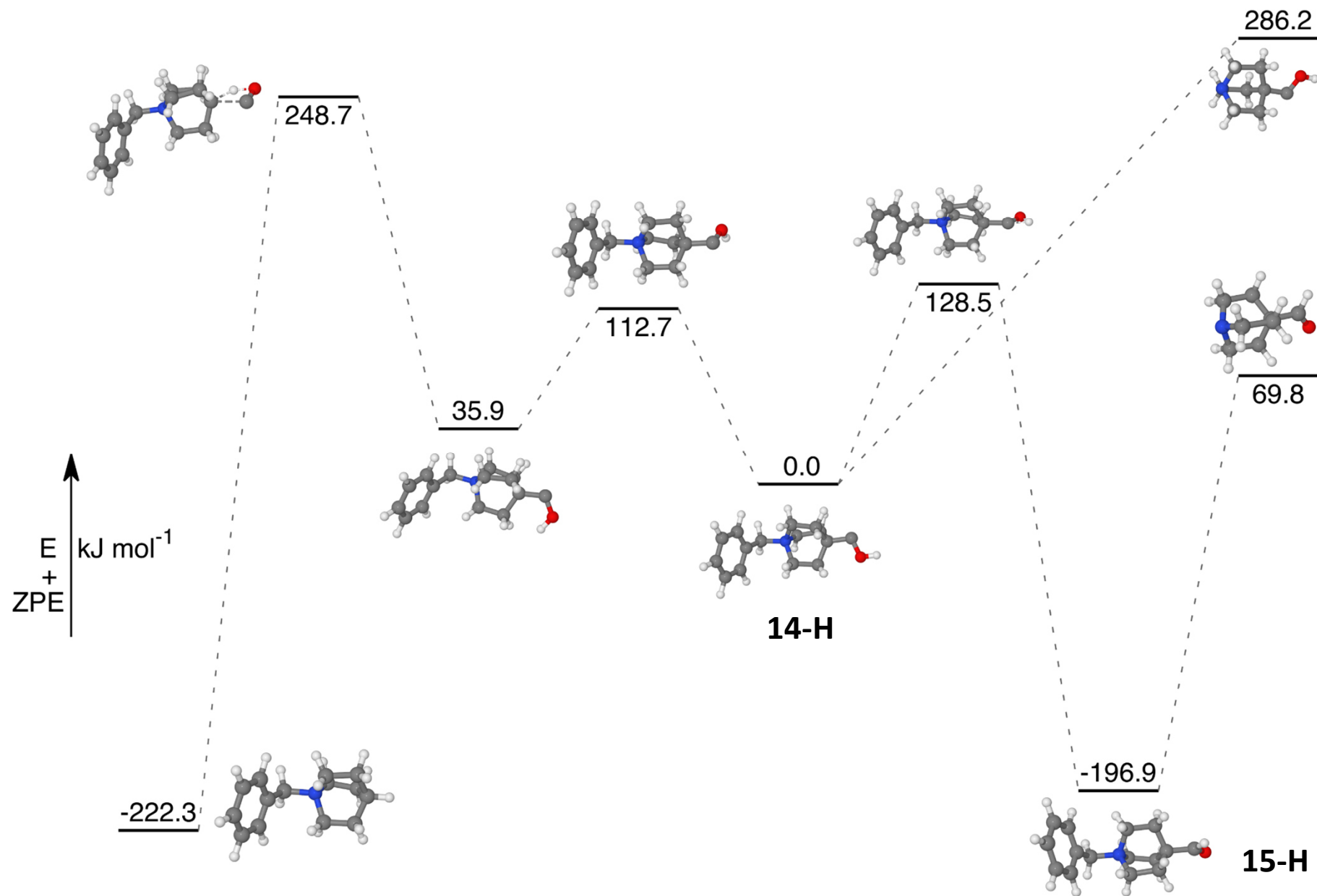
(a)

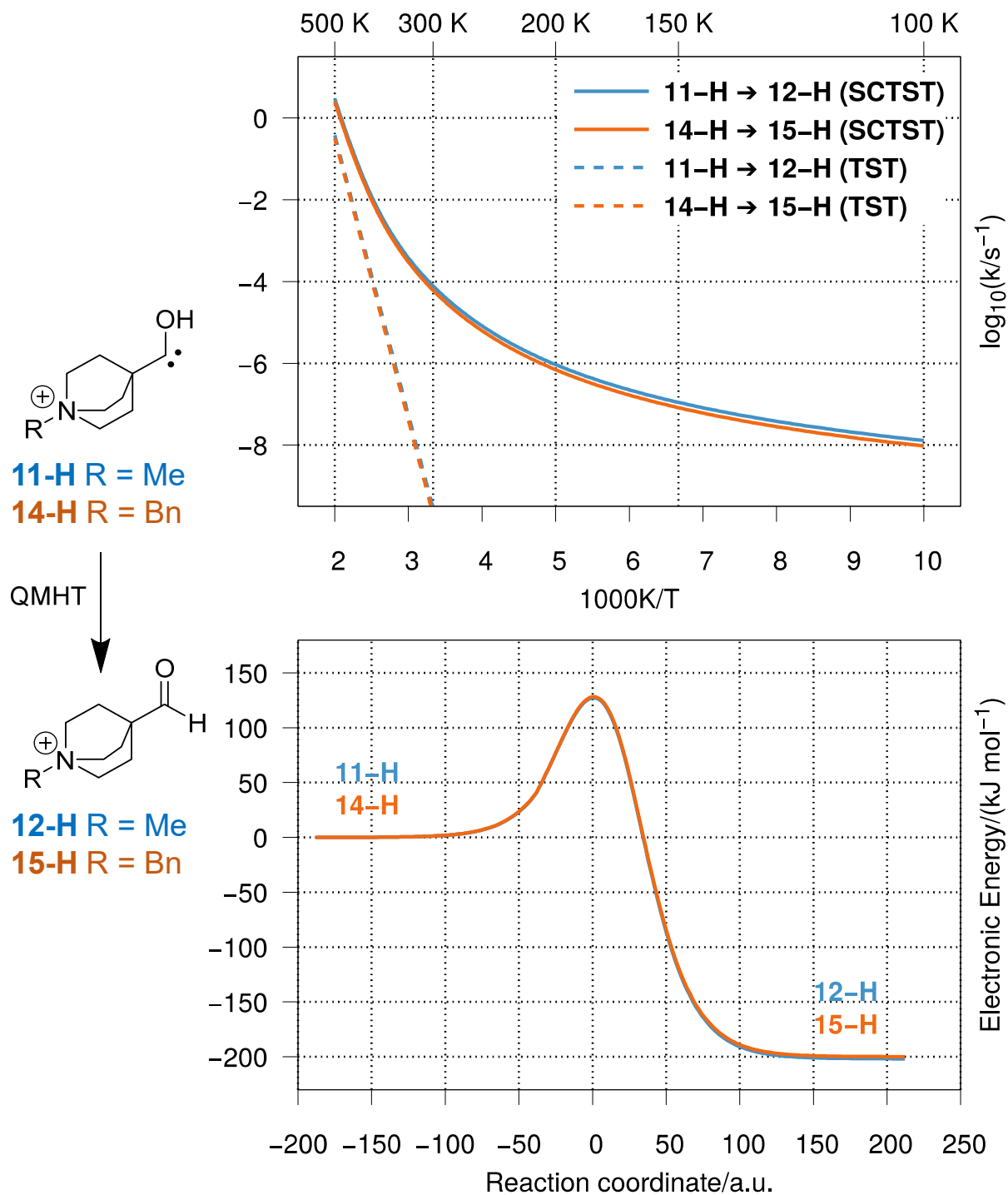


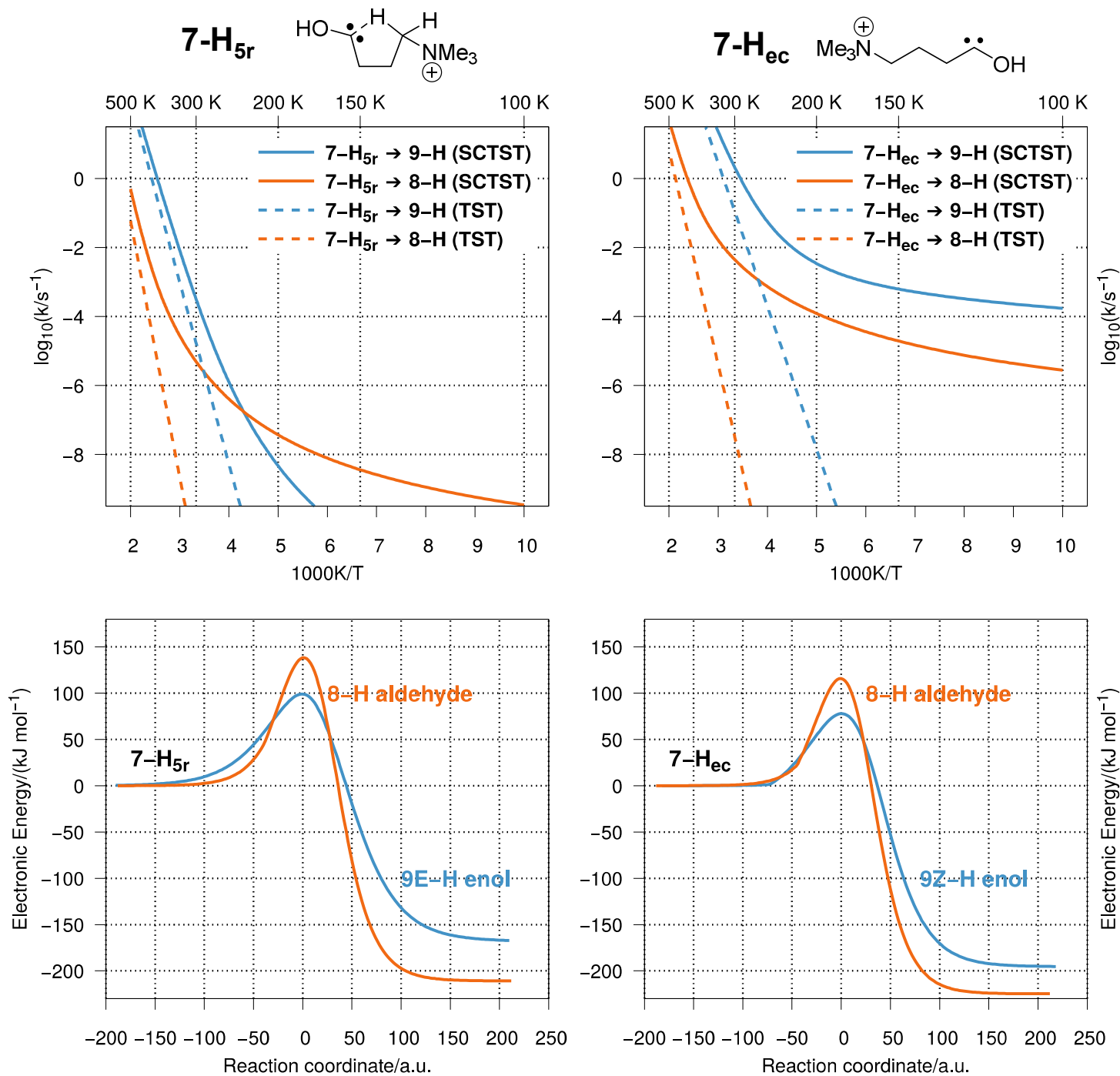
(b)

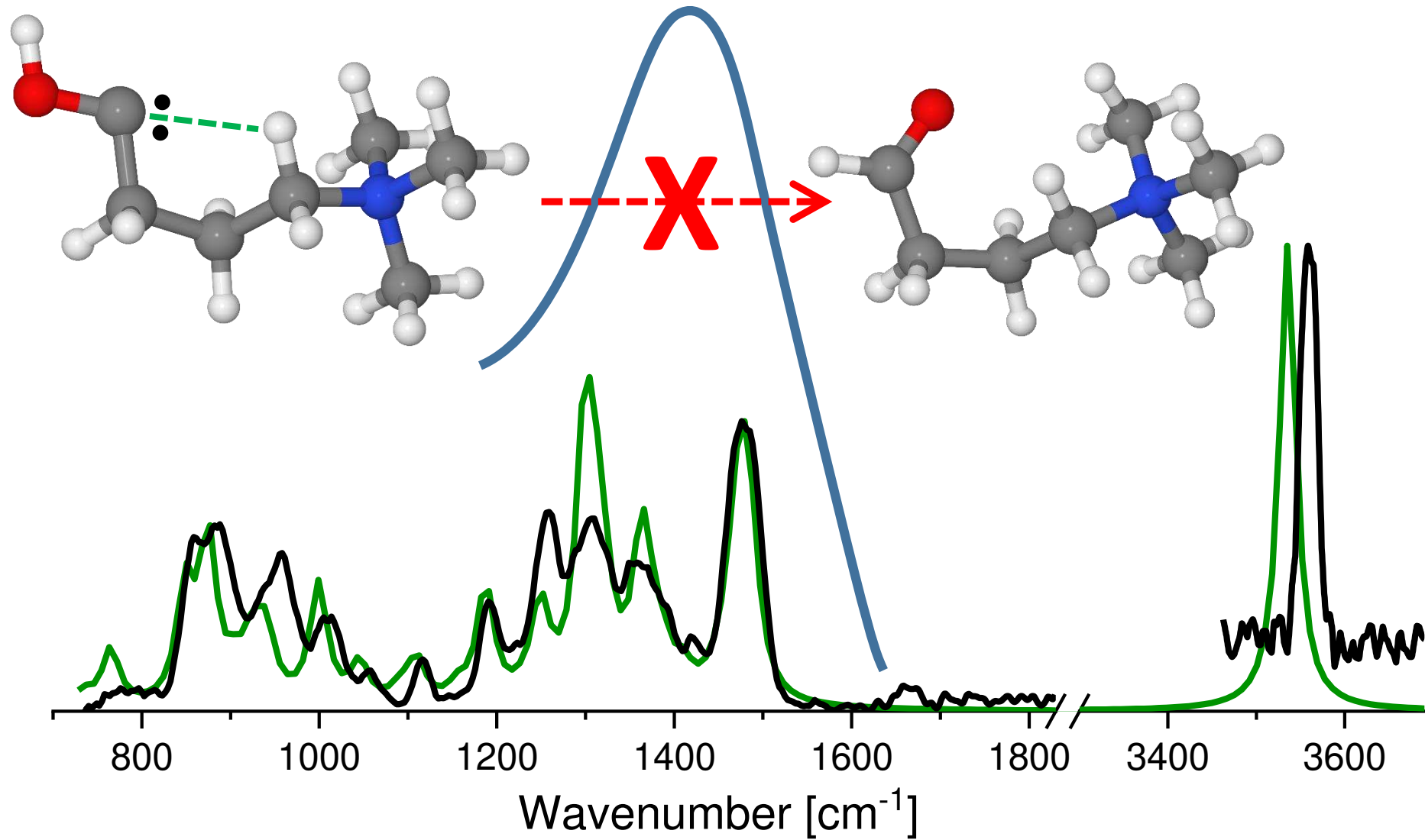












Caption

The aliphatic 3-(trimethylammonio)propylhydroxycarbene is stable in the gas phase and at room temperature performing no H-shift to *neither* aldehyde *nor* enol. As supported by DFT calculations, this QMHT inhibition is due to intramolecular H-bonding of the mildly acidic α -ammonio C-H bonds to the hydroxyl carbene's C-atom (C: \cdots H-C).